Published in final edited form as:
Inorg Chem. 2012 January 2; 51(1): 647–660. doi:10.1021/ic202094p.

Structural and Photophysical Properties of Visible– and Near–IR–Emitting Tris Lanthanide(III) Complexes Formed with the Enantiomers of *N*,*N*'–Bis(1–phenylethyl)–2,6–pyridinedicarboxamide

KimNgan T. Hua[†], **Jide Xu**[‡], **Eliseo E. Quiroz**[†], **Sabrina Lopez**[†], **Andrew J. Ingram**[†], **Victoria Anne Johnson**[†], **Angela R. Tisch**[†], **Ana de Bettencourt–Dias**[#], **Daniel A. Straus**[†], and **Gilles Muller**[†,*]

[1]San JoséState University, Department of Chemistry, 1 Washington Square, San José, California 95192–0101, United States

[2]University of California, Berkeley, Department of Chemistry, Berkeley, California 94720–1460, United States

[3]University of Nevada, Reno, Department of Chemistry, 1664 N. Virginia St., Reno, Nevada 89557–0216, United States

Abstract

The enantiomers of *N*,*N*'–bis(1–phenylethyl)–2,6–pyridinedicarboxamide (**L**), namely (*R*,*R*)–**1**, and (*S*,*S*)–**1**, react with Ln(III) ions to give stable $[Ln\mathbf{L}_3]^{3+}$ complexes in anhydrous acetonitrile solution and in the solid state, as evidenced by ES–MS, NMR and luminescence titrations, and their X–ray crystal structures, respectively. All $[Ln\mathbf{L}_3]^{3+}$ complexes (Ln(III) = Eu, Gd, Tb, Yb, and **L** = (*R*,*R*)–**1**, and (*S*,*S*)–**1**)) are isostructural and crystallize in the cubic space group I23. Although the small quantum yields of the Ln(III)–centered luminescence clearly point to the poor efficiency of the luminescence sensitization by the ligand and the intersystem crossing (ISC) and ligand–to–metal energy transfers, the ligand triplet–excited–state energy seems relatively well suited to sensitize many Ln(III) ion's emission, for instance, in the VIS (Eu, Tb), NIR (Nd, Yb), or in both regions (Pr, Sm, Dy, Er, Tm).

INTRODUCTION

Luminescent lanthanide(III), Ln(III), complex–based molecular probes are commonly employed for analytical and biomedical applications, where there are used either as diagnostic or as therapeutic tools.[1–25] Although it is now commonplace to use them in fields like biochemistry, biology, medicine, and related biomedical disciplines, there is still a considerable surge of interest to develop luminescent Ln(III) compounds possessing chiral properties in addition to their interesting spectral features. These unusual spectral characteristics often consist of, e.g., long excited–state lifetimes, line–like emission bands that are easily recognizable and well separated from the broad fluorescence bands of the

[*]**Corresponding Author** gilles.muller@sjsu.edu.

ASSOCIATED CONTENT

Supporting Information. ES–MS, NMR, and UV/VIS spectra/ data (Figs. S1, S3–S8, Tables S2, S11), luminescence sensitization determination, geometric optimization of the three optical isomers of **L** (Fig. S2), and all X–ray structural data (Figs. S9–S10, Tables S1, S3–S11) and CIF included files for all $[Ln\mathbf{L}_3]^{3+}$ compounds (Ln(III) = Eu, Gd, Tb, Yb, and **L** = (*R*,*R*)–**1** and (*S*,*S*)–**1**). This material is available free of charge via the Internet at http://pubs.acs.org.

organic fluorophores, large Stokes' shift, sensitivity to the local environment, or time–resolved separation between Ln(III) luminescence and short–lived background fluorescence.

Dipicolinic acid (H_2dpa) and its derivatives are good candidates for the design of luminescent Ln(III)–containing systems as evidenced, for instance, by their use for chirality sensing.[26] Since these 9–coordinate Ln(III) compounds exist as racemic mixtures of complexes with Δ and Λ helicity in solution, one can use them toward the molecular recognition of chiral biological substrates. This is possible due to the observation of induced chirality in the latter upon outer sphere coordination with a variety of optically active organic molecules such as tartrate substrates, amino acid or sugar derivatives,[26–32] a phenomenon referred to as the "Pfeiffer effect".[33] Of special importance, it was shown that the chiral recognition of such biomolecular substrates can be modulated by the nature of the ligand interface of the racemic 9–coordinate Ln(III) complexes.[34] More recently, it was reported that the chiroptical spectroscopic circularly polarized luminescence (CPL) technique, the emission analog to circular dichroism (CD), has potential for the chiral recognition of optical isomers of a given amino acid.[26, 27] This was possible because CPL is responsive to the nature and amount of the added chiral probes present in solution.

Since racemic Ln(III) complexes of ligands derived from dipicolinic acid are promising model systems for such studies and, also, that the modular nature of the dipicolinic acid's backbone allows for facile synthesis of derivatives with tunable photophysical and/or chiroptical properties,[35] we reported on the preparation of the optical isomers of *N*,*N*'–bis(1–phenylethyl)–2,6–pyridinedicarboxamide (**L**), namely (*R*,*R*)–**1** and (*S*,*S*)–**1**, and their Eu(III) complexes.[36] Of special importance, it was shown that these optical isomers of **L** formed stable 1:3 Eu(III):**L** complexes in anhydrous acetonitrile solution and resulted in a CPL activity independent of the "age" of the solution (e.g. several months) and a lack of noticeable photochemical degradation under continuous UV excitation (e.g. three days). In addition to these interesting features, these Eu(III)–containing compounds also possess chiroptical properties as evidenced by their CPL activity that may open new perspectives in the design of Ln(III) complexes acting as probes for chiral recognition, since they may probe the chirality of biomolecules by preferential interaction with one enantiomer. In particular, one can envisage that these Ln(III)–based systems with more extended structures and, also, containing chiral substituents may lead to a diastereomeric resolution of the 9–coordinate Ln(III) complexes, as already evidenced for the substituted pyridine–2,6–dicarboxamide ligand, $\mathbf{L^4}$, where a chiral group was grafted onto the *para*–position of the pyridine group.[37] Although this ligand led to the formation of stable 1:3 complexes with $\log\beta_3$ in the range 19–20, there was only a very small excess of one diastereoisomer induced in solution by $\mathbf{L^4}$. This was corroborated by a weak CPL activity of the Ln(III)–containing systems of interest. The calculated luminescence dissymmetry factor, g_{lum}, amounted to 0.02, a value much more smaller than those reported for the 9–coordinate Eu(III) complexes with the two optical isomers of **L**, (*R*,*R*,)–**1** and (*S*,*S*,)–**1**. (−0.19 and +0.19, respectively) or other related systems.[36–40]

In this paper we report on the interaction of the ligand **L** with trivalent Ln(III) ions with an emphasis on the structural, thermodynamic, and photophysical properties of the resulting tris complexes with Ln(III) ions emitting in the VIS and/or NIR regions. In addition to their potential use in chiral sensing applications, it is worth noting that such a study is of basic interest since the preliminary CPL results of the Eu(III)–containing complexes led to the suggestion that these latter can be employed as reliable CPL calibration standards to perform accurate routine tests of CPL instrumentation at low cost.[36]

EXPERIMENTAL SECTION

General

Solvents and starting materials were purchased from Acros or Sigma–Aldrich and used without further purification unless otherwise stated. Acetonitrile, dichloromethane, and methanol were purified in the usual way. Ln(III) trifluoromethanesulfonate, $Ln(Otf)_3$ (Ln(III) = La and Eu), were prepared from the lanthanum and europium oxides (Stanford Materials Corporation, 99.995%) and dried according to published procedures. The Ln content of solutions was determined by complexometric titrations with a standardized solution of ethylenediaminetetraacetic acid (EDTA) in the presence of 0.1 M ammonium acetate and arsenazo III. Unless otherwise specified, all sample solutions for the photophysical studies were prepared and stored in a glove box. The three isomers of **L**, (*R*,*R*, *S*,*S*, and *R*,*S*)–**1**, were synthesized as described previously.[36]

X–ray Experimental Section

Crystals suitable for X–ray analysis were mounted on a Kapton loop using Paratone N hydrocarbon oil and measured at low temperature using a Siemens SMART or APEX CCD[41] area detector with graphite monochromated Mo KR radiation (Tables 1 and S3 and S4). Cell constants and orientation matrices were obtained from least–squares refinement. The resulting data were integrated by the program SAINT[42] and corrected for Lorentz and polarization effects. Data were also analyzed for agreement and possible absorption using XPREP.[43] An empirical absorption correction based on the comparison of redundant and equivalent reflections was applied using SADABS.[44] Equivalent reflections where appropriate were merged, and no decay correction was applied. The structures were solved within the WinGX[45] package by direct methods using SIR2004[46] and expanded using a full–matrix least–squares techniques with SHELXL–97.[47] Hydrogen atoms were positioned geometrically for all H atoms. Resulting drawings of molecules were produced with ORTEP–3.[48] In the lattice of these complexes, there are a few unresolved disordered methanol and water molecules which were treated with the SQUEEZE routine included in PLATON;[49] the final refinement by this approach provided significantly better residuals.

Spectroscopic and Analytical Measurements

Optical rotation values were measured from 6.67×10^{-3} M solutions in anhydrous MeCN at 298 K with the help of a Rudolph Autopol III polarimeter (sodium D line). ^{1}H– and ^{13}C–NMR spectra and experiments ({^{1}H–^{1}H}COSY, {^{1}H–^{13}C}HSQC, and DEPT–135) were performed on a 300 MHz Mercury NMR spectrometer. Chemical shifts are given in ppm with respect to TMS. GC–MS data were obtained using an Agilent Technologies 6890N GC 5975B MSD instrument. Pneumatically–assisted electrospray mass spectra (ES–MS) were recorded from anhydrous acetonitrile solutions on an Agilent 6520 Q–TOF mass spectrometer by infusion at 0.5 $mL \cdot min^{-1}$. Elemental analyses were conducted at Desert Analytics, Inc (Tucson, AZ). Electronic spectra in the UV/VIS r1ange were recorded at 298 K with a Varian Cary 50 Bio UV–Visible Spectrophotometer with an attached Cary Single Cell Peltier Accessory for temperature control. Fluorescence at 298 K and above was measured on a Varian Cary Eclipse Fluorescence Spectrophotometer with an attached Quantum Northwest Temperature Control and/or on Horiba–Jobin–Yvon–IBH–FluoroLog–3 spectrofluorimeter, equipped with 3–slit double grating excitation and emission monochromators and a continuous wave 450 W xenon arc lamp as the light source for excitation. 77 K Phosphorescence scans were taken on a Perkin Elmer LS50B instrument. During luminescence titrations, a Masterflex® L/S® compact, variable speed pump was used with Chem–Durance Bio and Tygon Chemical 2001 tubing to transfer solutions to a 1.0 cm flow cuvette (Starna Cells, Inc.), and a Masterflex® L/S® Digital Drive with a Masterflex® L/S® Easy-Load® II pump head for precision tubing was used to automatically

dispense $Eu(NO_3)_3$ solutions. Luminescence lifetimes were determined with a Horiba–Jobin–Yvon–IBH–FluoroLog–3 spectrofluorimeter, adapted for time–correlated single–photon–counting (TCSPC) and multichannel scaling (MCS) measurements. A sub–microsecond Xe flashlamp (Jobin Yvon, 5000 XeF) was used as the light source, with an input pulse energy (100 nF discharge capacitance) of *ca*. 50 mJ, yielding an optical–pulse duration of less than 300 ns at FWHM. Emission was monitored perpendicular to the excitation pulse, using either a TBX–04–D (or R928P) detector in the UV–VIS region ('S' side) or a Hamamatsu H9170–75 PMT (or C9940–01 PMT) as the NIR detector ('T' side). For measurements in the UV–VIS region, spectral selection was achieved by passage through the double–grating emission monochromator (2.1 nm/mm dispersion, 1200 grooves/mm) and the spectra were corrected for emission spectral response (detector and grating). For measurements in the NIR, spectral selection was achieved by passage through a double grating emission monochromator (600 grooves/nm, 1 μm blaze), and the observed emission in this case was not corrected for the efficiency of the detector or grating. A thermoelectrically cooled single–photon–detection module (Horiba Jobin Yvon IBH, TBX–04–D) incorporating a fast–rise–time photomultiplier tube (PMT), a wide bandwidth preamplifier, and a picosecond constant–fraction discriminator was used as the detector. Signals were acquired with an IBH–DataStation–Hub photon–counting module in TCSPC mode, and data analysis was performed with the commercially available DAS–6 decay–analysis software package from Horiba Jobin Yvon IBH. Goodness of fit was assessed by minimizing the reduced chi squared function, χ^2, and a visual inspection of the weighted residuals. Each trace contained at least 10000 points, and the reported lifetime values resulted from at least three independent measurements.

The quantum yields (Φ) were measured by the optically dilute relative method[50] by use of the equation (1) where $\int_{Id\lambda}$ is the numerically integrated intensity from the luminescence spectra, *I* is the luminescent intensity at the excitation wavelength, *A* is the absorbance at the excitation wavelength, and *n* is the index of refraction of the solution. The subscript *R* denotes reference.

$$\frac{\Phi_{Sample}}{\Phi_R} = \left(\frac{\int I_{Sample} d\lambda}{\int I_R d\lambda} \right) \left(\frac{I_{R,exc}}{I_{Smaple,exc}} \right) \left(\frac{A_{R,\lambda_{exc}}}{A_{Sample,\lambda_{exc}}} \right) \left(\frac{n_{Sample}}{n_R} \right)^2 \quad (1)$$

Quantum yields of the ligand–centered emission were measured relative to quinine sulfate in 0.05 M H_2SO_4 (Q_{abs}=54.6%).[51] Quantum yields of the metal–centered emission were determined at excitation wavelengths at which (i) the Lambert–Beer law is obeyed and (ii) the absorption of the reference closely matches that of the sample. $Cs_3[Eu(DPA)_3]$ and $Cs_3[Tb(DPA)_3]$ in 0.1 M TRIS buffer were used as standards for the Eu(III) and Tb(III)–containing complexes (Q_{abs}=24.0 and 22.0%),[52] whereas quinine sulfate in 0.05 M H_2SO_4 and ligand **L** in MeCN were used as standards for $[Ln\mathbf{L}_n]^{3+}$ (Ln(III) = Nd, Sm, Gd, Dy, Er, and Yb). The complex $[Yb(tta)_3(H_2O)_2]$ (tta = thenoyltrifluoroacetylacetonate, Q_{abs}=0.35%) in toluene was also used as a standard for $[Yb\mathbf{L}_n]^{3+}$.[53] $Cs_3[Ln(DPA)_3]$ (Ln(III) = Eu and Tb) and $[Yb(tta)_3(H_2O)_2]$ were synthesized according to the published methods.[54, 55] The estimated error for quantum yields is ±10%.

Luminescence titrations were performed overnight with an automatic titration system where a solution containing 5.0×10^{-5} M **L**, as well as 0.05 M Et_4NClO_4 to maintain ionic strength, was constantly pumped back and forth from a sealed round–bottom flask and through a 10 mm quartz flow cuvette placed in the cell holder of a Varian Cary Eclipse Fluorescence Spectrophotometer set to scan every 15–18 minutes. At consistent time

intervals, a solution of 1.0×10^{-3} M $Ln(NO_3)_3$ (Ln(III) = Eu and Tb) in 0.05 M Et_4NClO_4 was dispensed into the **L** solution by an automatic peristaltic pump designed for precision. For each titration, at least 13 minutes were allowed for the solution in the flask to homogenize with that in the cuvette as well as allow for the Ln(III)–species to equilibrate. Factor analysis and stability constant determinations were carried out with the program Hyperquad2006.[56] All data reported are the average of three independent measurements. Computations were run on a Dell Precision 390 using the Spartan 06 program.[57]

Preparation of $[EuL_3]^{3+}$

0.097 g of **L** (0.25 mmol) and 0.030 g of $EuCl_3 \cdot 6H_2O$ (0.081 mmol) were added to a 50–ml round bottom flask. The mixture powder was then degassed by vacuum and the flask was placed under N_2 atmosphere. 5 ml of anhydrous methanol was added to the flask. The mixture was then stirred vigorously under nitrogen flow until the solution became clear. Liquid N_2 was used to freeze the solution and once again air was removed by vacuum. This step was repeated for three to five times and then filled the flask with N_2 again. The whole mixture was then refluxed under N_2 overnight at 328 K. After evaporating the solvent and drying the crude product, this latter was recrystallized by slow diffusion of *tert*–butyl methyl ether into a concentrated, hot and anhydrous MeOH solution to give 0.079 g of $[Eu\mathbf{L}_3]Cl_3$ (71%).

The other $[Ln\mathbf{L}_3]^{3+}$ complexes (Ln(III) = Eu, Gd, Tb, Yb, and **L** = (*R*,*R*)–**1** and (*S*,*S*)–**1**) were prepared in 50–71% yield according to the same procedure. Each of the complexes gave satisfactory elemental analyses. These elemental analyses were conducted on samples dried at about 313 K and under reduced pressure. It should be mentioned that a similar synthetic procedure was used to prepare $[Ln\mathbf{L}_3]^{3+}$ with (*R*,*S*)–**1**, but the elemental analyses suggested the formation of 1:2 species which were not characterized and studied further, since the purpose of this work was to study the formation of tris Ln(III) complexes and investigate their photophysical properties in solution.

$[Eu((R,R)–\mathbf{1})_3]Cl_3$. Yield 0.091 g, 71%. Anal. Calcd for $C_{69}H_{69}N_9O_6Cl_3Eu$: C, 60.1; H, 5.0; N, 9.1. Found: C, 60.0; H, 4.9; N, 9.2. ES–MS (MeCN): *m/z* 424.1 ($[Eu((R,R)–\mathbf{1})_3]^{3+}$).

$[Eu((S,S)–\mathbf{1})_3]Cl_3$. Yield 0.064 g, 50%. Anal. Calcd for $C_{69}H_{69}N_9O_6Cl_3Eu$: C, 60.1; H, 5.0; N, 9.1. Found: C, 60.1; H, 5.1; N, 9.3. ES–MS (MeCN): *m/z* 424.2 ($[Eu((S,S)–\mathbf{1})_3]^{3+}$).

$[Eu((R,R)–\mathbf{1})_3](CF_3SO_3)_3$. Yield 0.095 g, 60%. Anal. Calcd for $C_{72}H_{69}F_3N_9O_{15}S_3Eu$: C, 50.3; H, 4.0; N, 7.3. Found: C, 50.3; H, 3.7; N, 7.3. ES–MS (MeCN): *m/z* 424.2 ($[Eu((R,R)–\mathbf{1})_3]^{3+}$).

$[Eu((S,S)–\mathbf{1})_3](CF_3SO_3)_3$. Yield 0.082 g, 52%. Anal. Calcd for $C_{72}H_{69}F_3N_9O_{15}S_3Eu$: C, 50.3; H, 4.0; N, 7.3. Found: C, 50.2; H, 3.7; N, 7.3. ES–MS (MeCN): *m/z* 424.2 ($[Eu((S,S)–\mathbf{1})_3]^{3+}$).

$[Gd((R,R)–\mathbf{1})_3]Cl_3$. Yield 0.085 g, 66%. Anal. Calcd for $C_{69}H_{69}N_9O_6Cl_3Gd$: C, 59.9; H, 5.0; N, 9.1. Found: C, 59.7; H, 4.9; N, 9.0. ES–MS (MeCN): *m/z* 425.8 ($[Gd((R,R)–\mathbf{1})_3]^{3+}$).

$[Gd((S,S)–\mathbf{1})_3]Cl_3$. Yield 0.084 g, 65%. Anal. Calcd for $C_{69}H_{69}N_9O_6Cl_3Gd$: C, 59.9; H, 5.0; N, 9.1. Found: C, 59.8; H, 5.1; N, 8.9. ES–MS (MeCN): *m/z* 425.9 ($[Gd((S,S)–\mathbf{1})_3]^{3+}$).

$[Tb((R,R)–\mathbf{1})_3]Cl_3$. Yield 0.086 g, 66%. Anal. Calcd for $C_{69}H_{69}N_9O_6Cl_3Tb$: C, 59.8; H, 5.0; N, 9.1. Found: C, 59.8; H, 4.8; N, 9.2. ES–MS (MeCN): *m/z* 426.2 ($[Tb((R,R)–\mathbf{1})_3]^{3+}$).

$[Tb((S,S)–\mathbf{1})_3]Cl_3$. Yield 0.070 g, 54%. Anal. Calcd for $C_{69}H_{69}N_9O_6Cl_3Tb$: C, 59.8; H, 5.0; N, 9.1. Found: C, 59.7; H, 4.9; N, 9.0. ES–MS (MeCN): *m/z* 426.1 ($[Tb((S,S)–\mathbf{1})_3]^{3+}$).

[Yb((*R*,*R*)–**1**)$_3$]Cl$_3$. Yield 0.082 g, 63%. Anal. Calcd for $C_{69}H_{69}N_9O_6Cl_3Yb$: C, 59.2; H, 5.0; N, 9.0. Found: C, 59.4; H, 4.9; N, 9.0. ES–MS (MeCN): *m/z* 431.2 ([Yb((*R*,*R*)–**1**)$_3$]$^{3+}$).

[Yb((*S*,*S*)–**1**)$_3$]Cl$_3$. Yield 0.066 g, 51%. Anal. Calcd for $C_{69}H_{69}N_9O_6Cl_3Yb$: C, 59.2; H, 5.0; N, 9.0. Found: C, 59.1; H, 4.7; N, 9.3. ES–MS (MeCN): *m/z* 431.3 ([Yb((*S*,*S*)–**1**)$_3$]$^{3+}$).

RESULTS AND DISCUSSION

Structure of L

The synthesis of the three isomers of **L**, namely (*R*,*R*, *S*,*S*, and *R*,*S*)–**1**, was described in a preliminary report.[36] It was shown that the opposite optical rotation values of (*R*,*R*)–**1** and (*S*,*S*)–**1** (−213.4° and +213.6°, respectively) confirmed the chirality arising from the asymmetric carbons and the preparation of each enantiomeric form of **L**, while an optical rotation value of −0.8° for (*R*,*S*)–**1** corroborated the synthesis of the *meso* ligand with high purity. The room–temperature ^{1}H and ^{13}C–NMR spectra of the three isomers of **L** in CD_3CN and/or CD_2Cl_2, which display 6 and 10 signals respectively, are consistent with the presence of a single species having a C_{2v} symmetry: $X^{2,2'}$, $X^{3,3'}$, $X^{6,6'}$, $X^{7,7'}$ (X = C, H), $C^{5,5'}$, and $Ph^{8,8'}$ give rise to only one signal each. This is also corroborated by variable–temperature ^{1}H–NMR experiments, since the latter do not affect the signals of the various protons present in (*R*,*R*)–**1** and (*R*,*S*)–**1** (Fig. S1). The only significant shift observed is for the proton of the NH group moving upfield from ~8.2 to ~7.9 ppm with increasing temperature (253–328 K). Finally, the absence of a nuclear Overhauser effect between $H^{3,3'}$ and N–H points to a *syn*,*syn*,*ZZ* conformation for each isomer of **L**, as already reported for $\mathbf{L^8}$.[58]

This conformation also prevails in the solid state as evidenced by the X–ray crystal structure of the *meso*–isomer, (*R*,*S*)–**1** (Fig. 1). The unit cell contains two independent molecules A and B, the bond lengths and angles which differ only slightly (Tables 1 and S1). It is worth noting that such a *syn*,*syn*,*ZZ* conformation was already observed for 2,6–dicarboxamidopyridine derivatives[58–60] and is driven by the existence of two strong intramolecular hydrogen bonds involving the N atom of the pyridine ring and the NH portion of each carboxamide unit (NH…N(pyridine) = 2.33 and 2.29 Å or 2.34 and 2.35 Å for each independent molecule, respectively). The importance of these intramolecular hydrogen bonding interactions is evidenced by the observation of almost coplanar arrangements of the carboxamide side arms with the central pyridine ring (interplanar angles of 3.53(0.16)° and 3.63(0.15)° between C10–C9–O1–N1 or C14–C15–O2–N3 and C10–C14–N2, whereas the other independent molecule shows interplanar angles of 3.83(0.15)° and 6.39(0.14)°, respectively). Similarly, interplanar angles of 6.03(8) and 12.53(9)° and contact distances of 2.32 and 2.36 Å were reported for $\mathbf{L^8}$,[58] whereas ligand $\mathbf{L^9}$ showed an average interplanar angle of 24° with intramolecular hydrogen–bonding contact distances of 2.33–2.38Å.[59] It is worth noting that the structure of (*R*,*S*)–**1** does not reveal that each NH unit of one molecule interacts with one carbonyl oxygen of another molecule to form intermolecular hydrogen bonds, as it was evidenced for the two 2,6–dicarboxamidopyridine derivatives, $\mathbf{L^8}$ and $\mathbf{L^9}$.[58, 59]

Although we were not able to obtain suitable single X–ray–quality crystals for the two other isomers of **L**, (*R*,*R*)–**1** and (*S*,*S*)–**1**, their conformation predicted from gas–phase density functional theory (DFT) calculations, utilizing B3LYP[61, 62] and the 6–31G(d) basis set,[63, 64] pointed to a similar structural pattern than the X–ray crystal structure of (*R*,*S*)–**1**, namely a *syn*,*syn*,*ZZ* conformation, and, also, confirmed the enantiomeric nature of (*R*,*R*)–**1** and (*S*,*S*)–**1** (Fig. S2). It is worth noting that the predicted conformation from gas–phase molecular mechanics calculations and the resolved X–ray crystal structure for (*R*,*S*)–**1** are in good agreement with each other (Figs. 1 and S2). However, the predicted conformations show

that the two carbonyl groups in (*R*,*R*)–**1** and (*S*,*S*)–**1** are bent to opposite sides, whereas the two carboxamide O atoms are on the same side of the pyridine ring for the *meso*–isomer as evidenced in the X–ray crystal structure and predicted conformation of (*R*,*S*)–**1**. The position of the carboxamide O atoms in the *meso*–isomer is consistent with what was observed in $\mathbf{L}^{8}$,[58] but the interplanar angles are smaller (3.53(0.16) and 3.63(0.15)° or 3.83(0.15)° and 6.39(0.14)° *vs*. 6.03(8) and 12.53(9)°) and pointing to the fact that the carbonyls are even more in the plane with the pyridine ring than in $\mathbf{L}^{8}$.

Interaction Between L and Ln(III) Ions

Electrospray mass spectra (ES–MS) were recorded in order to probe the various Ln(III)–containing species that may be present in solution. Solutions of **L** (2×10^{-3} M in anhydrous MeCN, **L** = (*R*,*R*)–**1**) were titrated with either $Eu(NO_3)_3{\cdot}6H_2O$ or $Eu(CF_3SO_3)_3{\cdot}6H_2O$ at 298 K for ratios $R = [Eu]_t/[\mathbf{L}]_t = 0$–4. The spectra suggest the presence of $[Ln\mathbf{L}_n]^{3+}$ (n = 1–4) species, some of them with solvation molecules and/or in the form of nitrate/triflate adducts (Tables 2 and S2 and Fig. S3). Nitrate/triflate adducts and isotropic disctribution help in identifying the species, as shown in Fig. S4. Although the ES–MS analysis is only qualitative, it is worth noting that $[Ln\mathbf{L}_3]^{3+}$ is the most abundant species in the spectra of solutions with small *R* values, whereas solutions with larger *R* values show the coexistence of the latter species with $[Ln\mathbf{L}_2]^{3+}$ and $[Ln\mathbf{L}]^{3+}$. These data suggest the presence of the 1:1, 1:2, and 1:3 complexes in solution, as well as of a species with four ligands. Such species have been observed for ligands derived from, e.g., pyridine 2,6–dicarboxamide and bis(benzimidazole)pyridine, and were assigned to an outersphere association of a fourth ligand molecule with a 1:3 complex.[37, 65–67] However, it is most likely that such a species with four ligands is only formed during the ES–MS experiments, as corroborated by the luminescence (no effect on the fitting of the data) and NMR titrations (an excess of ligand only results in the presence of the 1:3 complex and free ligand, see below). More importantly, the ES–MS data indicate the presence of the 1:3 complex in solution since this latter is always observed in anhydrous acetonitrile solution and, also, represents the most abundant Ln(III)–containing species in solution at every *R* value.

To confirm these observations and, also, to quantitatively characterize the formation of complexes with **L**, luminescence titrations of **L** with $Eu(NO_3)_3{\cdot}6H_2O$ at 298 K in anhydrous MeCN, in the presence of 0.05 M Et_4NClO_4, and under N_2 atmosphere were performed. Taking account of the species identified in the ES–MS and NMR spectra (see below for NMR discussion), the luminescence data (Figs. S5 and S6) were fitted with non–linear least–squares methods to equilibria (2)–(4), where solvation and anion coordination were omitted.

$$Eu^{3+} + \mathbf{L} \rightleftharpoons [Eu\mathbf{L}]^{3+} \quad \log\beta_1 \tag{2}$$

$$Eu^{3+} + 2\,\mathbf{L} \rightleftharpoons [Eu\mathbf{L}_2]^{3+} \quad \log\beta_2 \tag{3}$$

$$Eu^{3+} + 3\,\mathbf{L} \rightleftharpoons [Eu\mathbf{L}_3]^{3+} \quad \log\beta_3 \tag{4}$$

Although the factor analysis indicates the presence of three or four emitting species, a model including $[Eu\mathbf{L}_4]^{3+}$ does not improve the fit, in agreement with the postulated outer–sphere nature of this species detected in the gas phase. Close examination of the time–resolved luminescence data shows that plots of luminescence intensity *vs*. the ratio $R = [Eu]_t/[\mathbf{L}]_t$ at several wavelengths (Fig. S7) have essentially two breaks at R = 0.33 and 0.5 (1:3 and 1:2 complexes). The cumulative stability constants are summarized in Table 3.

The logβ_3 value of the Eu(III) complex (23.8) is in good agreement with those reported for corresponding compounds with 2,6–dicarboxamidopyridine derivatives (e.g. 22.3, 19.7, and 17.6 for **L**^{5}, **L**^{4}, and **L**^{6}).[37, 58, 68] Of special importance, it confirms that the steric hindrances resulting from the wrapping of the tridentate strands play a predominant role in the formation of the triple–helical complexes [Ln**L**$^{i}_3$]$^{3+}$ (*i* = 5–8).[58, 68] It was shown that the bulkiness of the terminal tertiary amide groups resulted in increased interstrand steric repulsions and, consequently, destabilized significantly the stability of the 1:3 complex (the logβ_3 values were lowered by several orders of magnitude) to the point where the formation of this species was not observed.[58] In this latter case, the terminal dibenzylamine groups in **L**^{7} precluded the formation of 1:3 species due to their bulkiness, and only resulted in the observation of 1:1 and 1:2 species. However, the removal of two benzyl groups led to the formation of tris complexes as evidenced by the crystal structure of [Tb(**L**^{8})$_3$]$_2$(CF$_3$SO$_3$)$_6$, but it was a slow process in solution due to the existence of several inert conformational isomers resulting from the blocked rotations around the OC–N bonds.[58] This slow complexation process ascribed from the stabilization of the ligand **L**^{8} in its *syn*,*syn*,*ZZ* conformation and, as a result, strongly limited its characterization in solution. The replacement of the benzyl groups of the carboxamide units by phenylethyl substituents with respect to **L**^{7} confirmed the formation of tris complexes with **L** (**L** = (*R*,*R*)–**1** and (*S*,*S*)–**1**) in the solid state (see below), but also in solution (logβ_3 of 23.8). This can be attributed to the fact that in **L**^{8} the replacement of one of the two H atoms of the benzyl group by a Me substituent probably results in a smaller activation energy barrier for the rotation about the OC–N bonds (steric hindrances due to the presence of the Me group) and, therefore, **L** (**L** = (*R*,*R*)–**1** and (*S*,*S*)–**1**) is not locked in its *syn*,*syn*,*ZZ* conformation as seen for **L**^{8}. Thus, the two intramolecular NH…N(pyridine) hydrogen bonds, which led to the formation of a blocked *syn*,*syn*,*ZZ* conformation for **L**^{8},[58] are weakened and do not prevent the formation of stable 1:3 complexes with **L** (**L** = (*R*,*R*)–**1** and (*S*,*S*)–**1**) in solution (a faster complexation reaction is favored) as evidenced by the luminescence titrations and ^{1}H–NMR spectra.

The speciation and, in particular, the formation of stable 1:3 species with **L** (**L** = (*R*,*R*)–**1** and/or (*S*,*S*)–**1**) in solution under anhydrous conditions was confirmed by monitoring the titration of (*R*,*R*)–**1** with La(III) by ^{1}H–NMR at 298 K (Fig. 2). The successive formation of the three complexes, namely 1:1, 1:2, and 1:3, were observed for ratios, R =[La]$_t$/[**L**]$_t$, going from 0.33, 0.5 to 1.0. When R reaches 0.33, all ligands are complexed and are in the 1:3 species, whereas the solutions with R = 1.0 and 0.5 show the various La(III)–containing species (1:1 and 1:2, and 1:1, 1:2 and 1:3, respectively). It is worth noting that no free ligand is observed in solution for the various ratios (within the experimental error) confirming the successive formation of the three Ln(III)–containing compounds with **L**. Addition of more ligand (R = 0.2) validated these observations since the ^{1}H–NMR spectrum of this solution only showed the 1:3 species and the excess of free ligand. A similar situation was also observed for Eu(III) (Fig. S8). The observation of only one set of signals for each complex in these ^{1}H–NMR spectra corroborates that **L** (**L** = (*R*,*R*)–**1** and/or (*S*,*S*)–**1**) adopts an *anti*–*anti* conformation upon complexation to the Ln(III) ions, but also that the solution contains only one major diastereoisomer of [Ln**L**$_3$]$^{3+}$ (either Λ–[Ln((*R*,*R*)–**1**)$_3$]$^{3+}$ or Δ–[Ln((*S*,*S*)–**1**)$_3$]$^{3+}$, see below for further details), as already seen in several other studies on complexes with, i.e., chiral tertendate ligands derived from terpyridine (**L**^{1}), bis(benzimidazole)pyridine (**L**^{2} and **L**^{3}) or 2,6–pyridinedicarboxamide (**L**^{4} and **L'**), and chiral octadentate 1–hydroxy–2–pyridinone (1,2–HOPO) and 2–hydroxyisophthalamide (IAM)–based ligands.[37, 39, 65, 69–71] A similar conclusion was also drawn from the CPL measurements.[36, 38] It was found that the strong CPL activity exhibited by [Eu**L**$_3$]$^{3+}$ (e.g. g_{lum} value amounted to −0.19 at 590 nm for **L** = (*R*,*R*)–**1**) is comparable when either a direct excitation of the Eu(III) ion in the spectral range of the ^{5}D$_0$→^{7}F$_1$ transition or an indirect excitation through the ligand absorption bands was used but also is independent of the polarization of the excitation beam (e.g. right–, left–, or plane–polarized light). This was

consistent with the presence of only one diastereomeric species in solution.[27, 28, 38, 71, 72] On the other hand, one would have expected that the CPL would have been dependent on the excitation polarization if the solution would have contained a mixture of diastereoisomers.[73, 74] This is also in good agreement with the X–ray crystal structures of $[Ln\mathbf{L}_3]^{3+}$ (Ln(III) = Eu, Gd, Tb, Yb and **L** = (*R*,*R*)–**1** and (*S*,*S*)–**1**) showing the formation of triple helical complexes in the solid state (see below). In summary, the apparent easy formation of the 1:3 species contrasts with what was observed with **L**[8],[58] and confirms that **L** is not blocked in the *syn*,*syn*,*ZZ* conformation. Additionally, these ^{1}H–NMR experiments confirmed that a solution of the 1:3 species can be prepared *in situ* by mixing a MeCN solution of the Ln(III) salt with one of **L** in a Ln(III):**L** molar ratio of 1:3 and under anhydrous conditions.

Isolation, Characterization, and Structure of $[LnL_3]^{3+}$

The 1:3 complexes were obtained under the form of microcrystalline powders in 50–71% yield from the diffusion of *tert*–butyl methyl ether into concentrated, hot, and anhydrous MeOH solutions containing **L** (**L** = (*R*,*R*)–**1** and (*S*,*S*)–**1**) and $LnX_3{\cdot}xH_2O$ (Ln(III) = Eu, Gd, Tb, Yb, X = Cl^-, NO_3^-, and/or $CF_3SO_3^-$, and *x* = 5 or 6) in a molar ratio of 3.1:1. The isolated $[Ln\mathbf{L}_3]^{3+}$ complexes (Ln(III) = Eu, Gd, Tb, and Yb) yielded good elemental analysis and dissolution in anhydrous MeCN gave ES–MS and/or ^{1}H–NMR data similar to those obtained from complex solutions prepared *in situ* with a Ln(III):**L** molar ratio of 1:3 or 1:5. It is worth noting that the high resolution $^5D_0 \leftarrow {}^7F_0$ excitation spectra of the Eu(III)–containing complex solution formed *in situ* under nonanhydrous conditions confirmed that the Eu(III) ions were in the form of the 1:3 species in a 6.67×10^{-3} M MeCN solution with a stoichiometric 1:5 ratio.[36] Taking account of these observations, some of the $[Ln\mathbf{L}_3]^{3+}$ (Ln(III) = Pr, Nd, Sm, Dy, Er, and Tm) complexes were not isolated, but only prepared *in situ* using anhydrous conditions for the purpose of the photophysical studies. These solutions were prepared in the glove box using a Ln(III):**L** ratio of 1:5 to ensure that only the 1:3 complex species was present in solution, since it was observed in a previous study that a ratio of 1:3 resulted in the presence of 1:2 and 1:3 complex species in solution when nonanhydrous conditions were used.[36]

Single crystals suitable for X–ray diffraction analysis were obtained for the $[Ln\mathbf{L}_3]^{3+}$ (Ln(III) = Eu, Gd, Tb, and Yb) complexes with the two enantiomeric forms of **L**, (*R*,*R*)–**1** and (*S*,*S*)–**1**. The details of the crystallographic data collection are summarized in Tables 1, S3, and S4. All complexes are isostructural and crystallize in the cubic space group I23. The unit cell contains isolated $[Ln\mathbf{L}_3]^{3+}$ cations with disordered noncoordinated solvent molecules and chloride anions, which explain the fractional values found (see Experimental section). All Ln(III) ions are coordinated by six carboxamide O atoms and three pyridine N atoms. The structure of the different $[Ln\mathbf{L}_3]^{3+}$ (Ln(III) = Eu, Gd, Tb, Yb, and **L** = (*R*,*R*)–**1** and (*S*,*S*)–**1**) cations with the atom–numbering scheme are display in Figures 3–4 and S9–S10 and selected bond lengths and angles are reported in Tables 4 and S5–S10, while selected interplanar angles are listed in Tables S11. In each cation, the three ligand molecules are meridionally coordinated to and in a helical way around the Ln(III) ion leading to the observation of almost ideal D_3–like complexes for the four Ln(III)–containing species. This is corroborated by equivalent Ln–X bond lengths and X–Ln–Y angles (X = N, O and Y = N, O) for each of the three ligand molecules coordinated to the Ln(III) cation. It is worth noting that the average Ln–X distances become shorter along the studied Ln(III) ion series (Eu–Yb). For instance, the Ln–N(Pyridine) distance in $[Ln\mathbf{L}_3]^{3+}$ is decreasing from 2.564(2), 2.543(2), 2.528(2) to 2.467(2) Å for Ln(III) = Eu, Gd, Tb, Yb and **L** = (*R*,*R*)–**1**, respectively. A similar pattern was observed for the 1:3 species with the other enantiomeric form of **L**, (*S*,*S*)–**1**. One can conclude from these observations that the coordination cavity is modular and fits Ln(III) ions of various sizes such as Eu(III) or Yb(III). Both X–ray crystal

structures of Eu(III) and Yb(III) only show slightly differences in the interplanar angles between the carboxamide side arms and the central pyridine ring (5.86(0.12) and 7.35(0.16)° *vs*. 4.16(0.12) and 6.75(0.14)° for **L** = (*R*,*R*)–**1**), whereas the angle between the ligand strand planes is very similar (75.28 *vs*. 76.76°), respectively. It is also evidenced by the slightly smaller values of the effective ionic radius (1.09, 1.08, 1.07, and 1.01) of the Ln(III) ions (Ln = Eu, Gd, Tb, Yb and **L** = (*R*,*R*)–**1** and (*S*,*S*)–**1**), calculated according to Shannon's definition with *r*(N) = 1.46 and *r*(O) = 1.31 Å,[75] from the expected ionic radii for nine–coordinated Ln(III) ions (1.12, 1.07, 1.095, and 1.042Å), respectively. These smaller values are due to a slight contraction of the Ln(III) coordination sphere which is induced by the wrapped of the three tridentate ligand molecules, as already reported for $[Eu\mathbf{L}^{5}_{3}]^{3+}$ (1.09 vs. 1.12Å).[68]

Moreover, the average Ln–N(Pyridine) and Ln–O(amide) bonds of 2.56 or 2.54 and 2.40 or 2.38 Å are close to those found in the related Ln(III) complexes (Ln = Eu or Tb) with carboxamide ligand derivatives, respectively.[68, 76] The crystal packing is governed by intramolecular (C1–C6 phenyl ring with C10–C14–N2 central pyridine ring of another ligand strand, but in the same complex molecule) and intermolecular (C1–C6 phenyl ring with C18–C23 phenyl ring of another complex molecule) π–stacking interactions and weak intermolecular H–bonding interactions between the Cl atom of the noncoordinated chlorides and the amide H atom or the O atom of the noncoordinated solvent molecules (Fig. 5).

Finally, it should be added that the asymmetric carbon atoms of the ligands retain their absolute configuration *R* or *S* in all the complex cations. Thus, the Δ or Λ metal stereochemistry is induced by the chiral nature of the ligand molecules in all of the complexes studied by X–ray crystallography. That is, ligand (*S*,*S*)–**1** induces a Δ chirality about the Ln(III) ions, whereas ligand (*R*,*R*)–**1** induces a Λ chirality about the Ln(III) ions. These findings, which confirm the diastereomeric nature of $[Ln\mathbf{L}_3]^{3+}$ with (*R*,*R*)–**1** and (*S*,*S*)–**1**, are also in agreement with those reported for related highly symmetrical isostructural chiral 1:3 Ln(III) complexes with a chiral pyridyldiamide ligand derivative, pyridine–2,6–dicarboxylic acid bis–[(1–naphthalen–1–yl–ethyl)–amide] (**L'**). This ligand only differs from **L** by its carboxamide moieties in which the phenyl groups of **L** are replaced by naphthalene substituents.[39] It is also worth noting that the diastereomeric nature of $[Ln\mathbf{L}_3]^{3+}$ with (*R*,*R*)–**1** and (*S*,*S*)–**1** also prevails in solution as evidenced by the CPL results from the Eu(III)–containing species (observation of mirror–image CPL spectra that are independent of the polarization of the excitation beam and if a direct or indirect excitation is used).[36, 38] A complete study of the chiroptical properties of these compounds of interest will be described in a forthcoming publication. [77]

Ligand–Centered Emission

The electronic spectrum of **L** in solution displays a broad band defined by two broad maxima around 276 and 284 nm, and assigned to $n\rightarrow\pi^*$ and $\pi\rightarrow\pi^*$ transitions centered onto the pyridine–dicarboxamide units (Figure S11). UV irradiation of **L** at room temperature yields one broad unresolved fluorescence band, centered around 337 nm, and originating from the $^1\pi\pi^*$ state (Fig. 6). At 77 K, the fluorescent band is more structured and emission from the $^3\pi\pi^*$ state appears with a maximum around 391 nm. As one would expect, the findings for both enantiomeric forms of **L**, (*R*,*R*)–**1** and (*S*,*S*)–**1**), are identical within the experimental error. Thus, we only report the photophysical data for one of them thereafter with **L** meaning either (*R*,*R*)–**1** or (*S*,*S*)–**1**). The same practice is applied to the discussion of the photophysical properties of the $[Ln\mathbf{L}_3]^{3+}$ complexes.

Upon complexation to Gd(III) in the 1:3 complex, the broad band observed in the electronic spectrum of **L** is only slightly red-shifted with the appearance of two broad maxima around 277 and 286 nm. Similar results were obtained for the other $[Ln\mathbf{L}_3]^{3+}$ complexes

investigated (Fig. S11). On complexation to the nonluminescent Gd(III) ion, the transitions of the $^1\pi\pi^*$ and $^3\pi\pi^*$ states are red–shifted by 175 and 885 cm^{-1}, respectively (frozen MeCN solution, 77 K, see Fig. 6). These changes in the position of the $^1\pi\pi^*$ and $^3\pi\pi^*$ states between the free and complexed ligands confirm the formation of the complex. On the other hand, one can also envisioned that the localization of the 0–phonon of the $^3\pi\pi^*$ state of the complexed ligand in the Gd(III)–containing compound at 27025 cm^{-1} (or 370 nm) is well suited to sensitize many Ln(III) ions emitting, for instance, in the VIS (Eu, Tb), NIR (Nd, Yb), or in both regions (Pr, Sm, Dy, Er, Tm).

Eu and Tb–Centered Luminescence

The luminescence spectra of $[Eu\mathbf{L}_3]^{3+}$ and $[Tb\mathbf{L}_3]^{3+}$ were recorded in MeCN solutions at a concentration of 10^{-3} M which represents a compromise between decomplexation and self–quenching. According to the stability constants determined for $[Eu\mathbf{L}_n]^{3+}$ in MeCN (n = 1–3, Table 3), about 99% of the species present in solution for a stoichiometric ratio Eu:**L** of 1:3 is under the form of $[Eu\mathbf{L}_3]^{3+}$ (ligand speciation).

Excitation via the ligand–centered $n,\pi\rightarrow\pi^*$ transitions of $[Eu\mathbf{L}_3]^{3+}$ and $[Tb\mathbf{L}_3]^{3+}$ result in the observation of the typical luminescence spectra of Eu(III) and Tb(III) with sharp line emission bands arising from the $^5D_0$ and $^5D_4$ excited states on the ^7F_J manifold ground states (J = 0–6 and 6–0), respectively (Fig. 6). It can been seen that these luminescence spectra of $[Eu\mathbf{L}_3]^{3+}$ and $[Tb\mathbf{L}_3]^{3+}$ also show the residual emission of the ligand–centered $^1\pi\pi^*$ and $^3\pi\pi^*$ states, suggesting incomplete intersystem crossing (ISC) and ligand–to–Ln(III) energy transfers, respectively. These poor energy conversion processes are confirmed by the relatively modest to small quantum yields of both the ligand– and metal–centered luminescence measured at RT, and the ratio between the integrated $^3\pi\pi^*$ and $^1\pi\pi^*$ state emissions, $I^{(T)}/I^{(S)}$ for the free ligand and its Gd(III) complex at 77 K.

The quantum yield of $[Gd\mathbf{L}_3]^{3+}$ (Φ^F = 2.2%) decreases by a factor of 10 with respect to that of the free ligand (Φ^F = 21.2%), whereas the ligand–centered phosphorescence increases, as indicated by the 10–fold increase of $I^{(T)}/I^{(S)}$ from 4.0×10^{-3} to 4.7×10^{-2} on complexation of **L** to with Gd(III). This better ISC efficiency in the Gd(III) complex may probably result from a more favorable energy gap between the $^1\pi\pi^*$ and $^3\pi\pi^*$ states, $\Delta E(^3\pi\pi^*–^1\pi\pi^*)$ = 5070 cm^{-1}, as compared to 4190 cm^{-1} in the free ligand (optimal ISC energy transfer process needs to have a $\Delta E(^3\pi\pi^*–^1\pi\pi^*)$ greater than 5000 cm^{-1}),[78] and from the mixing of the ligand–centered $^1\pi\pi^*$ and $^3\pi\pi^*$ wavefunctions promoted by spin–orbit and/or paramagnetic effects.[79, 80]

The overall quantum yield of the Ln(III)–centered luminescence obtained upon ligand excitation, $\Phi^{Ln}{}_L$, amounts to 1.0% for $[Eu\mathbf{L}_3]^{3+}$, as compared to 8.6% for the corresponding compound with Tb(III). This 9–fold difference may probably be explained by the fact that (i) Eu(III) has a tendency to favor the quenching of the singlet excited state of the sensitizing chromophore (a process usually not observed for Tb(III) since it is very difficult to reduce this ion), (ii) the possibility of having an energy transfer in the Tb(III) compounds from the ligand triplet state to a higher metal electronic state (i.e. $^5D_3$) than the emissive state of Tb(III), $^5D_4$ (the higher metal state is populated and then undergoes a rapid internal conversion and vibrational relaxation to the emissive metal state $^5D_4$), and (iii) a better efficiency of the ligand–to–metal energy transfer.[81, 82] The energy gap between the $^3\pi\pi^*$ state of the complexed ligand and the excited state of Tb(III), $^5D_4$, is closer, although relatively large ($\Delta E(^3\pi\pi^*–^5D_4)$ = 6535 cm^{-1}) to the ideal value of 2500–3500 cm^{-1} for an efficient ligand–to–metal energy transfer,[78] than the one for $[Eu\mathbf{L}_3]^{3+}$ ($\Delta E(^3\pi\pi^*–^5D_0)$ = 9800 cm^{-1}). One can conclude that the small quantum yields of the Ln(III)–centered luminescence clearly point to the poor efficiency of the ISC and ligand–to–metal energy transfers. Another factor that may also largely contribute to relatively modest quantum

yields of the Eu(III) and Tb(III) complexes is the weak efficiency of the luminescence sensitization by the ligand ($\eta_{sens} = 4.0 \times 10^{-5}$, see Supporting Information for a detailed determination of this value). However, the slight decrease in the Eu($^5D_0$) and Tb($^5D_4$) lifetimes from 1.84 and 1.95 to 1.75 and 1.89 ms between 77 K and RT suggests that temperature–dependent quenching mechanisms (e.g. energy back transfer, ligand–to–metal charge transfer, or other intermolecular interactions…) do not significantly contribute to the nonradiative deactivation processes responsible for the fairly small Ln(III)–centered luminescence quantum yields of $[Eu\mathbf{L}_3]^{3+}$ and $[Tb\mathbf{L}_3]^{3+}$. The long Eu($^5D_0$) and Tb($^5D_4$) lifetimes also suggest that the metallic site in $[Eu\mathbf{L}_3]^{3+}$ and $[Tb\mathbf{L}_3]^{3+}$ is efficiently protected from external interactions (e.g. no solvent molecules present in the first coordination sphere) due to the helical arrangement of the three ligand molecules around the Ln(III) ion. This is in line with the NMR data since these latter do not point to a partial decomplexation of one of the arms of the coordinated ligand molecules through the binding of a solvent molecule. A similar phenomenon was reported for MeCN solutions of analogous 1:3 complexes with a ligand derived from pyridine 2,6–dicarboxamide ($\mathbf{L}^4$) for which Eu($^5D_0$) and Tb($^5D_4$) lifetime values of 1.58 and 1.55 ms were observed.[37] It is interesting to note that the quantum yields for $[Eu(\mathbf{L})_3]^{3+}$ and $[Tb(\mathbf{L})_3]^{3+}$ are 4.5 and 7.2 times larger than those for $[Ln(\mathbf{L}^4)_3]^{3+}$ (0.22 and 1.2%) despite larger $\Delta E(^3\pi\pi^*–^5D_0)$ and $\Delta E(^3\pi\pi^*–^5D_4)$ energy gaps (9800 and 6535 *vs*. 8000 and 4850 cm^{-1}). This can be explained by the fact that $\mathbf{L}^4$ itself is essentially nonluminescent and is only weakly luminescent in the compounds with La and Lu ($\Phi^F = 5.5 \times 10^{-2}$ and 6.5×10^{-2}%),[37] whereas the quantum yields of **L** and its Gd(III) complex amount to 21.2 and 2.2%, respectively. It is also worth pointing out that the Ln–containing compounds with ligands incorporating carboxamide moieties generally exhibit weaker luminescence than those with carboxylic groups. In addition to the effect on the electronic and structural properties, the carboxamide–carboxylate substitution significantly affects the efficiency of the energy transfer processes and, in particular, the sensitization process. Although a generalization would be difficult, it seems that this latter is improved in systems containing carboxylate groups.[58, 67, 68, 83]

Pr, Nd, Sm, Dy, Er, Tm, and, Yb–Centered Luminescence

Since the ligand triplet–excited–state energy seems well suited to populate most of the Ln(III) ions, we prepared all the complexes $[Ln\mathbf{L}_3]^{3+}$ with the Ln(III) cations emitting from the *f–f* orbitals and yielding sensitization of Pr, Nd, Sm, Dy, Er, Tm, and, Yb. With the exception of Nd and Yb that only emit in the NIR region, all of them possess transitions in the VIS and NIR regions. The luminescence spectra for complexes $[Ln\mathbf{L}_3]^{3+}$ (Ln(III) = Pr, Nd, Sm, Dy, Er, Tm, and, Yb) are plotted in Fig. 7. The luminescence quantum yields and lifetimes in MeCN solutions were measured, when possible, and are discussed thereafter. Below we discuss briefly the feature of these VIS– and NIR–emitting Ln(III)–complexes. It is worth mentioning that the assignment of the Ln(III)–centered VIS and NIR luminescence bands of the systems of interest is consistent with what one would expect from such Ln(III)–containing compounds.[7, 84]

Luminescence spectra of $[Nd\mathbf{L}_3]^{3+}$ and $[Yb\mathbf{L}_3]^{3+}$ after excitation into the ligand–centered $n,\pi\rightarrow\pi^*$ transitions display typical narrow–band emission in the NIR region. Three characteristic emission bands are observed for $[Nd\mathbf{L}_3]^{3+}$ at about 890, 1056, and 1340 nm, which correspond to the $^4F_{3/2}\rightarrow{}^4I_J$ (J = 9/2, 11/2, and 13/2) *f–f* transitions of the Nd(III) ion. Similarly, one structured and one broad emission bands are observed for $[Yb\mathbf{L}_3]^{3+}$ and $[Er\mathbf{L}_3]^{3+}$ around 977 and 1511 nm, corresponding to the $^2F_{5/2}\rightarrow{}^2F_{7/2}$ and $^4I_{13/2}\rightarrow{}^4I_{15/2}$ transitions of Yb(III) and Er(III), respectively. It is worth noting that the observation of a structured emission band for $[Yb\mathbf{L}_3]^{3+}$ may be attributed to the crystal–field or stark splitting as already reported for other Yb(III)–based systems. [85–88] Although Er(III) is known for having VIS emission bands,[7] the luminescence spectrum of $[Er\mathbf{L}_3]^{3+}$ in the VIS

region is dominated by the broad emission from the complexed ligand. It is worthwhile noting that the luminescence spectra of $[Ln\mathbf{L}_3]^{3+}$ (Ln(III) = Pr, Sm, Dy, and Tm) reveal the characteristic emission bands of Pr(III), Sm(III), Dy(III), and Tm(III) in the VIS and NIR regions upon excitation via the ligand–centered $n,\pi\rightarrow\pi^*$ transitions. [7] The assignment of the emission observed from the $[Pr\mathbf{L}_3]^{3+}$ complex is more complicated compared with other Ln(III) ions, since Pr(III) can emit from three different excited states, namely the $^3P_0$, $^1D_2$, and $^1G_4$ levels. Accordingly, the luminescence spectrum of $[Pr\mathbf{L}_3]^{3+}$ shows the characteristic VIS emission bands of Pr(III) at about 488, 604, and 650 nm, which can be attributed to the $^3P_0\rightarrow{}^3H_4$, $^1D_2\rightarrow{}^3H_4$, and $^3P_0\rightarrow{}^3F_2$ transitions. The presence of the luminescence peaks of $^1D_2\rightarrow{}^3H^4$ (604 nm) and $^3P_0\rightarrow{}^3F_2$ (650 nm) in the spectrum of $[Pr\mathbf{L}_3]^{3+}$ confirms that the ligand triplet–excited–state energy is relatively well positioned to populate the $^3P_0$ level of Pr(III), which is located at about 21000 cm^{-1} (or 476 nm). This is in line with other published data for which the absence of these two luminescence peaks led to the conclusion that the position of the $^3\pi\pi^*$ state of the ligand in the Pr(III) complexes was too low to populate the $^3P_0$ level of Pr(III) effectively. [89, 90] Thus, the VIS luminescence spectra of these Pr(III)–containing compounds only showed the emission band of the $^3P_0\rightarrow{}^3H_4$ transition at about 490 nm. On the other hand, the observed NIR emission bands in the luminescence spectrum of $[Pr\mathbf{L}_3]^{3+}$ at 1028 and 1450 nm can be assigned to the $^1D_2\rightarrow{}^3F_4$ and $^1D_2\rightarrow{}^1G_4$ transitions.[91] Under the same conditions, the luminescence spectrum of $[Sm\mathbf{L}_3]^{3+}$ displays the typical VIS $^4G_{5/2}\rightarrow{}^6H_{5/2}$, $^6H_{7/2}$, $^6H_{9/2}$, and $^6H_{11/2}$ and NIR $^4G_{5/2}\rightarrow{}^6F_{5/2}$, $^6F_{7/2}$, and $^6F_{9/2}$ transitions centered at 561, 603, 644, and 710 and 950, 1030, and 1206 nm, respectively. Although the luminescence of $[Tm\mathbf{L}_3]^{3+}$ is very weak, the characteristic Tm(III) emission from the $^1G_4$ level is observed with the VIS $^1G_4\rightarrow{}^3H_6$ and $^3H_4$ (478 and 650 nm) and NIR $^1G_4\rightarrow{}^3F_4$ transitions (1125 nm). Finally, the luminescence spectrum of $[Dy\mathbf{L}_3]^{3+}$ displays the characteristic VIS (480, 573, and 660 nm) and NIR (1000, 1148, and 1310 nm) emission bands, and corresponding to the $^4F_{9/2}\rightarrow{}^6H_J$ (J =15/2, 13/2, 11/2, and 9/2) and $^4F_{5/2}\rightarrow{}^6F_J$ (J = 3/2 and ½) transitions, respectively.

Furthermore, time–resolved luminescence measurements showed that the observed luminescence lifetimes of the complexes $[Ln\mathbf{L}_3]^{3+}$ (Ln(III) = Nd, Sm, Dy, and Yb) in MeCN at RT are in the range of microseconds, with the Yb(III) and Nd(III) compounds having the shortest lifetimes and the Sm(III) and Dy(III) complexes the longest (0.6, 51.4, 45.1, and 4.2 μs). The lifetimes and/or luminescence spectra of $[Ln\mathbf{L}_3]^{3+}$ (Ln(III) = Pr, Er, and Tm) were too short and/or too weak to be measured with our instrumental setup. However, it is not surprising that $[Sm\mathbf{L}_3]^{3+}$ and $[Dy\mathbf{L}_3]^{3+}$ have much shorter luminescence lifetimes than their corresponding compounds with Eu(III) and Tb(III), since the Ln(III) ions with smaller energy gaps (e.g. Dy and Sm) are quenched more efficiently than those with larger energy gaps (e.g. Eu and Tb).[90, 92, 93] The vibrational deactivation of the luminescent state by OH and/or XH (X = N or C) oscillators is more efficient when the energy gap between the luminescent–state and ground–state manifolds is small. It is also worth noting that the absolute quantum yields of $[Ln\mathbf{L}_3]^{3+}$ (Ln(III) = Nd, Sm, Dy, Er, and Yb) determined in MeCN upon ligand excitation are much smaller (1.4×10^{-2}, 2.4×10^{-2}, 1.0×10^{-1}, 3.5×10^{-5}, and 1.9×10^{-3}%, see Experimental Section) than those of $[Eu\mathbf{L}_3]^{3+}$ and $[Tb\mathbf{L}_3]^{3+}$ (1.0 and 8.6%) since their luminescence signal is affected by additional vibrational quenching processes, as already pointed out during the lifetime discussion. It is worth mentioning that these observations are consistent with other published data.[74, 94, 95] As stated earlier, the nonradiative deactivation processes are amplified for Ln(III) ions with small energy gaps, and even more accentuated for NIR–emitting Ln(III)–complexes.[90, 92, 93, 96] However, the overall weak Ln(III)–centered NIR luminescence of $[Ln\mathbf{L}_3]^{3+}$ is also due to the poor efficiency of the energy transfer processes within the ligand bands (ISC) and between the ligand and the Ln(III) ions. This is evidenced by the observation of the complexed ligand's emission in the VIS region of the luminescence spectra of these systems of interest (Fig. 7).

CONCLUSIONS

Contrary to **L**[8],[58] the optical isomers of **L**, namely (*R*,*R*)–**1** and (*S*,*S*)–**1**, restored the formation of stable tris complexes in anhydrous acetonitrile solution, as evidenced by $\log\beta_3$ values in the range of 23.8. The replacement of the benzyl groups of the carboxamide units in **L**[8] by phenylethyl substituents revealed that **L** was not locked in a *syn,syn,ZZ* conformation as seen for **L**[8]. This can be attributed to the steric hindrances resulting from the replacement of one of the two H atoms of the benzyl group in **L**[8] by a Me substituent and, consequently, leading to a smaller activation energy barrier for the rotation about the OC–N bonds. In addition to the formation of isostructural $[Ln\mathbf{L}_3]^{3+}$ complexes for the Ln(III) series studied (Eu–Yb) in the solid state, the introduction of a chiral asymmetric carbon in each carboxamide moiety led to a diastereomeric resolution of the 9–coordinate Ln(III) complexes. Of special importance, the Δ or Λ metal stereochemistry was induced by the chiral nature of the ligand ((*S*,*S*)–**1** or (*R*,*R*)–**1**), respectively.

In addition to these findings supported by the structural and spectroscopic studies performed, it was also shown that the ligand triplet–excited–state energy was relatively well suited to sensitize many Ln(III) ions emitting in the VIS and/or NIR regions. Although the sensitization of these Ln(III) ions was relatively weak due to poor energy transfer processes, one can envision to use these stable $[Ln\mathbf{L}_3]^{3+}$ complexes for their chiroptical properties (i.e. large CPL activities observed)[36, 38, 77] to develop reliable empirical relationships between chiral structures and CPL sign patterns. Of special importance, one may be able to develop a "helicity rule" aimed at determining a Δ or Λ helicity configuration based upon CPL sign patterns from such Ln(III)–containing systems or related compounds emitting in the VIS and NIR regions. Research in these directions is currently underway.

It is also interesting to note that studies on Ln(III) complexes with C_4–symmetrical chiral tetraamide derivative ligands based on 1,4,7,10–tetraazacyclododecane may suggest that there is a correlation between the sign of the torsional angle NCCO or NCCN and the metal stereochemistry.[97, 98] It was shown that an (*R*)–configuration at the C center resulted in negative and positive signs for the ring NCCO and C_4–related NCCN torsion angles, associated with Λ and δ configurations, respectively. A similar behavior was found for C_3–symmetric Ln(III) complexes of a pyridylphenylphosphinate triazacyclononane based ligand even though this ligand did not exhibit chirality about an amide moiety.[99] In this case an (*R*)–configuration at the P atom results in positive and negative signs for the ring NCCN and substituent $NCCN_{py}$ torsion angles, associated with an Λ configuration. Although it is premature to conclude that a similar phenomenon applies to D_3–like symmetric Ln(III) compounds such as those with **L** and **L'**, one may wonder if, e.g, a negative NCXO or NCCN torsion angle is generally associated with an (*R*)–configuration. However, it is worth pointing out that the same behavior was observed in each of these Ln(III)–containing systems. That is, Δ or Λ stereochemistry about Ln(III) was selectively induced by ligand chirality. This potential for a priori selection of metal stereochemistry will continue to be explored in the forthcoming years.

Supplementary Material

Refer to Web version on PubMed Central for supplementary material.

Acknowledgments

The authors thank Dr. Christopher M. Andolina for assistance with lifetime measurements. We also thank Prof. Kenneth N. Raymond of University of California, Berkeley for the use of his spectrofluorometer, adapted for time–correlated single–photon–counting (TCSPC) and multichannel scaling (MCS) measurements. Similarly, Prof. Ana de Bettencourt–Dias of University of Nevada, Reno is thanked for the use of her instrumentation to perform

measurements in the NIR region during G.M.'s one–semester visiting position in her research group. G.M. thanks the National Institute of Health, Minority Biomedical Research Support (1 SC3 GM089589–02 and 3 S06 GM008192–27S1) and the Henry Dreyfus Teacher–Scholar Award for financial support, whereas the NSF MRI Grant No. 0923573 is thanked for the use of the San José State University Protein Laboratory. E.E.Q. and S.L. thank the NIH RISE Grant No. 5R25GM071381 for research fellowships. A.J.I. thanks the Howard Hughes Medical Institute Award (52006312) for a research fellowship and the 2010 Claudia Greathead Research Stipend at San José State University. A.d.B.D. thanks the University of Nevada, Reno and the National Science Foundation (CHE 0733458) for financial research support.

REFERENCES

1. Shinoda S, Tsukube H. Analyst. 2011; 136:431–435. [PubMed: 21170445]
2. Ye Z, Chen J, Wang G, Yuan J. Anal. Chem. 2011; 83:4163–4169. [PubMed: 21548628]
3. Fung YO, Wu W, Yeung C-T, Kong H-K, Wong KK-C, Lo W-S, Law G-L, Wong K-L, Lau C-K, Lee C-S, Wong W-T. Inorg. Chem. 2011; 50:5517–5525. [PubMed: 21591737]
4. Hagan AK, Zuchner T. Anal. Bioanl. Chem. 2011; 400:2847–2864.
5. Wang X, Wang X, Wang Y, Guo Z. Chem. Commun. 2011; 47:8127–8129.
6. Liu X, Ye Z, Wei W, Du Y, Yuan J, Ma D. Chem. Commun. 2011; 47:8139–8141.
7. Bünzli J-CG. Chem. Rev. 2010; 110:2729–2755. [PubMed: 20151630]
8. Bünzli J-CG. Chem. Letters. 2009; 38:104–109.
9. Moore EG, Samuel APS, Raymond KN. Acc. Chem. Res. 2009; 42:542–552. [PubMed: 19323456]
10. Bünzli J-CG, Comby S, Chauvin A-S, Vandevyver CDB. J. Rare Earths. 2007; 25:257–274.
11. Bünzli, J-CG. Metal Ions in Biological Systems. In: Sigel, A.; Sigel, H., editors. Metal Complexes in Tumor Diagnosis and as Anticancer Agents. Vol. Vol. 42. New York: Marcel Dekker Inc.; 2004. p. 39-75.
12. Poole RA, Kielar F, Richardson SL, Stenson PA, Parker D. Chem. Commun. 2006:4084–4086.
13. Bünzli, J-CG. Rare Earth Luminescent Centers in Organic and Biochemical Compounds. In: Liu, G.; Jacquier, B., editors. Spectroscopic Properties of Rare Earths in Optical Materials. Vol. Vol. 83. Berlin: Springer; 2005. p. 462-499.
14. Parker D, Yu J. Chem. Commun. 2005:3141–3143.
15. Pal R, Parker D. Org. Biomol. Chem. 2008; 6:1020–1033. [PubMed: 18327327]
16. Tremblay MS, Lee M, Sames D. Org. Lett. 2008; 10:5–8. [PubMed: 18069839]
17. Hemmilä I, Mukkala VM. Crit. Rev. Clin. Lab. Sci. 2001; 38:441–519.
18. Chauvin A-S, Comby S, Song B, Vandevyver CDB, Bünzli J-CG. Chem. Eur. J. 2008; 14:1726–1739. [PubMed: 18098236]
19. Bünzli J-CG, Chauvin A-S, Vandevyver CDB, Bo S, Comby S. Ann. N.Y. Acad. Sci. 2008; 1130:97–105. [PubMed: 18596338]
20. Chauvin A-S, Comby S, Song B, Vandevyver CDB, Thomas F, Bünzli J-CG. Chem. Eur. J. 2007; 13:9515–9526. [PubMed: 17879248]
21. Law G-L, Wong K-L, Man CW-Y, Wong W-T, Tsao S-W, Lam MH-W, Lam PK-S. J. Am. Chem. Soc. 2008; 130:3714–3715. [PubMed: 18321106]
22. Song B, Vandevyver CDB, Deiters E, Chauvin A-S, Hemmilä I, Bünzli J-CG. Analyst. 2008; 133:1749–1756. [PubMed: 19082079]
23. Yam VW-W, Lo KK-W. Coord. Chem. Rev. 1998; 184:157–240.
24. Andraud C, Maury O. Eur. J. Inorg. Chem. 2009:4357–4371.
25. Ma Y, Wang Y. Coord. Chem. Rev. 2010; 254:972–990.
26. Muller G. Dalton Trans. 2009:9692–9707. (Invited Perspective Article). [PubMed: 19885510]
27. Riehl, JP.; Muller, G. Circularly Polarized Luminescence Spectroscopy and Emission-Detected Circular Dichroism. In: Berova, N.; Polavarapu, PL.; Nakanishi, K.; Woody, R., editors. Comprehensive Chiroptical Spectroscopy. John Wiley & Sons, Inc.; in press
28. Riehl, JP.; Muller, G. Circularly Polarized Luminescence Spectroscopy from Lanthanide Systems. In: Gschneidner, KA., Jr; Bünzli, J-CG.; Pecharsky, VK., editors. Handbook on the Physics and

Chemistry of Rare Earths. Vol. Vol. 34. Amsterdam: North-Holland Publishing Company; 2005. p. 289-357.

29. Tsukube H, Shinoda S. Chem. Rev. 2002; 102:2389–2403. [PubMed: 12059273]
30. Parker D, Dickins RS, Puschmann H, Crossland C, Howard JAK. Chem. Rev. 2002; 102:1977–2010. [PubMed: 12059260]
31. Brittain HG. J. Coord. Chem. 1989; 20:331–347.
32. Brittain HG. Pract. Spectrosc. 1991; 12:179–200.
33. Kirschner S. J. Indian Chem. Soc. 1974; LI:28–31.
34. Moussa A, Pham C, Bommireddy S, Muller G. Chirality. 2009; 21:497–506. [PubMed: 18698640]
35. George MR, Golden CA, Grossel MC, Curry RJ. Inorg. Chem. 2006; 45:1739–1744. [PubMed: 16471988]
36. Bonsall SD, Houcheime M, Straus DA, Muller G. Chem. Commun. 2007; 35:3676–3678.
37. Muller G, Schmidt B, Jiricek J, Hopfgartner G, Riehl JP, Bünzli J-CG, Piguet C. J. Chem. Soc. Dalton Trans. 2001:2655–2662.
38. Do K, Muller FC, Muller G. J. Phys. Chem. A. 2008; 112:6789–6793. [PubMed: 18597442]
39. Leonard JP, Jensen P, McCabe T, O'Brien JE, Peacock RD, Kruger PE, Gunnlaugsson T. J. Am. Chem. Soc. 2007; 129:10986–10987. [PubMed: 17696537]
40. Yuasa J, Ohno T, Miyata K, Tsumatori H, Hasegawa Y, Kawai T. J. Am. Chem. Soc. 2011; 133:9892–9902. [PubMed: 21598978]
41. SMART, version 5.059: Area-Detector Package. Madison, WI: Bruker Analytical X-ray Systems, Inc.; 1999.
42. SAINT, version 7.07B: SAX Area-Detector Integration Program. Madison, WI: Siemens Industrial Automation, Inc.; 2005.
43. XPREP, version 6.12: Part of the SHELXTL Crystal Structure Determination Package;. Madison, WI: Bruker AXS Inc.; 1995.
44. Sheldrick, GM. SADABS, version 2.10: Siemens Area Detector Absorption Correction Program. Göttingen, Germany: University of Göttingen; 2005.
45. Farrugia LJ. WinGX 1.70.01. J. Appl. Crystallogr. 1999; Vol. 32:837–838.
46. Burla MC, Caliandro R, Camalli M, Carrozzini B, Cascarano GL, De Caro L, Giacovazzo C, Polidori G, Spagna R. J. Appl. Crystallogr. 2005; 38:381–388.
47. Sheldrick, GM. SHELX97, Programs for Crystal Structure Analysis. Institut fur Anorganische Chemie der Universitat: Gottingen, Germany; 1998.
48. Farrugia LJ. J. Appl. Crystallogr. 1997; 30:565.
49. Spek, AL. PLATON-A Multipurpose Crystallographic Tool. Utrecht, The Netherlands: Utrecht University; 2007.
50. Demas JN, Crosby GA. J. Phys. Chem. 1971; 75:991–1024.
51. Meech SR, Phillips DC. J. Photochem. 1983; 23:193–217.
52. Chauvin A-S, Gumy F, Imbert D, Bünzli J-CG. Spectrosc.Lett. 2004; 37:517–532.
53. Meshkova SB, Topilova ZM, Bolshoy DV, Beltyukova SV, Tsvirko MP, Venchikov VY. Acta Phys. Pol. A. 1999; 95:983–990.
54. Brayshaw PA, Bünzli J-CG, Froidevaux P, Harrowfield JM, Kim Y, Sobolev AN. Inorg. Chem. 1995; 34:2068–2076.
55. Charles RG, Ohlmann RC. J. Inorg. Nucl. Chem. 1965; 27:255–259.
56. Gans P, Sabatini A, Vacca A. Talanta. 1996; 43:1739–1753. [PubMed: 18966661]
57. Shao Y, Molnar LF, Jung Y, Kussmann J, Ochsenfeld C, Brown ST, Gilbert ATB, Slipchenko LV, Levchenko SV, O'Neill DP, DiStasio RA Jr, Lochan RC, Wang T, Beran GJO, Besley NA, Herbert JM, Lin CY, Van Voorhis T, Chien SH, Sodt A, Steele RP, Rassolov VA, Maslen PE, Korambath PP, Adamson RD, Austin B, Baker J, Byrd EFC, Dachsel H, Doerksen RJ, Dreuw A, Dunietz BD, Dutoi AD, Furlani TR, Gwaltney SR, Heyden A, Hirata S, Hsu C-P, Kedziora G, Khalliulin RZ, Klunzinger P, Lee AM, Lee MS, Liang W, Lotan I, Nair N, Peters B, Proynov EI, Pieniazek PA, Rhee YM, Ritchie J, Rosta E, Sherrill CD, Simmonett AC, Subotnik JE, Woodcock HL III, Zhang W, Bell AT, Chakraborty AK, Chipman DM, Keil FJ, Warshel A, Hehre WJ,

Schafer HL III, Kong J, Krylov AI, Gill PMW, Head-Gordon M. Phys. Chem. Chem. Phys. 2006; 8:3172–3191. [PubMed: 16902710]

58. Le Borgne T, Bénech J-M, Floquet S, Bernardinelli G, Aliprandini C, Bettens P, Piguet C. Dalton Transactions. 2003:3856–3868.
59. Malone JF, Murray CM, Dolan GM. Chem. Mater. 1997; 9:2983–2989.
60. Meghdadi S, Nalchigar S, Khavasi HR. Acta Cryst. 2008; E64:o431.
61. Becke AD. J. Chem. Phys. 1993; 98:1372–1377.
62. Becke AD. J. Chem. Phys. 1993; 98:5648–5652.
63. Petersson GA, Bennett A, Tensfeldt TG, Al-Laham MA, Shirley WA, Mantzaris J. J. Chem. Phys. 1988; 89:2193–2218.
64. Petersson GA, Al-Laham MA. J. Chem. Phys. 1991; 94:6081–6090.
65. Muller G, Riehl JP, Schenk KJ, Hopfgartner G, Piguet C, Bünzli J-CG. Eur. J. Inorg. Chem. 2002:3101–3110.
66. Muller G, Bünzli J-CG, Schenk KJ, Piguet C, Hopfgartner G. Inorg. Chem. 2001; 40:2642–2651. [PubMed: 11375674]
67. Renaud F, Piguet C, Bernardinelli G, Bünzli J-CG, Hopfgartner G. Chem. Eur. J. 1997; 3:1660–1667.
68. Renaud F, Piguet C, Bernardinelli G, Bünzli J-CG, Hopfgartner G. Chem. Eur. J. 1997; 3:1646–1659.
69. Muller G, Maupin CL, Riehl JP, Birkedal H, Piguet C, Bünzli J-CG. Eur. J. Inorg. Chem. 2003:4065–4072.
70. Muller G, Bünzli J-CG, Riehl JP, Suhr D, von Zelewsky A, Mürner H. Chem. Commun. 2002:1522–1523.
71. Seitz M, Moore EG, Ingram AJ, Muller G, Raymond KN. J. Am. Chem. Soc. 2007; 129:15468–15470. [PubMed: 18031042]
72. Samuel APS, Lunkley JL, Muller G, Raymond KN. Eur. J. Inorg. Chem. 2010:3343–3347. [PubMed: 20730030]
73. Seitz M, Do K, Ingram AJ, Moore EG, Muller G, Raymond KN. Inorg. Chem. 2009; 48:8469–8479. [PubMed: 19639983]
74. D'Aléo A, Xu J, Do K, Muller G, Raymond KN. Helv. Chim. Acta. 2009; 92:2439–2460. [PubMed: 20161476]
75. Shannon RD. Acta Crystallogr. 1976; A32:751–767.
76. Tanase S, Gallego PM, de Gelder R, Fu WT. Inorg. Chim. Acta. 2007; 360:102–108.
77. Hua KT, Lopez S, Ponce SG Jr, Muller G. manuscript in preparation.
78. Steemers FJ, Verboom W, Reinhoudt DN, van der Tol EB, Verhoeven JW. J. Am. Chem. Soc. 1995; 117:9408–9414.
79. Tobita S. J. Phys. Chem. 1985; 89:5649–5654.
80. Tobita S, Arakawa M, Tanaka I. J. Phys. Chem. 1984; 88:2697–2702.
81. Parker D. Coord. Chem. Rev. 2000; 205:109–130.
82. Parker D, Williams JAG. J.Chem.Soc. Dalton Trans. 1996:3613–3628.
83. Senegas J-M, Bernardinelli G, Imbert D, Bünzli J-CG, Morgantini P-Y, Weber J, Piguet C. Inorg. Chem. 2003; 42:4680–4695. [PubMed: 12870960]
84. Quici S, Cavazzini M, Marzanni G, Accorsi G, Armaroli N, Ventura B, Barigelletti F. Inorg. Chem. 2005; 44:529–537. [PubMed: 15679381]
85. Chen X-Y, Yang X, Holliday BJ. Inorg. Chem. 2010; 49:2583–2585. [PubMed: 20163123]
86. Mato-Iglesias M, Rodríguez-Bias T, Platas-Iglesias C, Starck M, Kadjane P, Ziessel R, Charbonnière L. Inorg. Chem. 2009; 48:1507–1518. [PubMed: 19149468]
87. Kang T-S, Harrison BS, Bouguettaya M, Foley TJ, Boncella JM, Schanze KS, Reynolds JR. Adv. Funct. Mater. 2003; 13:205–210.
88. Gonçalves e Silva FR, Malta OL, Reinhard C, Güdel H-U, Piguet C, Moser JE, Bünzli JCG. J. Phys. Chem. A. 2002; 106:1670–1677.

89. Moore EG, Szigethy G, Xu J, Pålsson L-O, Beeby A, Raymond KN. Angew. Chem. Int. Ed. 2008; 47:9500–9503.
90. Davies GM, Aarons RJ, Motson GR, Jeffrey JC, Adams H, Faulkner S, Ward MD. Dalton Trans. 2004:1136–1144. [PubMed: 15252652]
91. Dang S, Yu J, Wang X, Sun L, Deng R, Feng J, Fan W, Zhang H. J. Lumin. 2011; 131:1857–1863.
92. Haas Y, Stein G, Würzberg E. J. Chem. Phys. 1974; 60:258–263.
93. Wolbers MPO, van Veggel FCJM, Snellink-Ruël BHM, Hofstraat JW, Geurts FAJ, Reinhoudt DN. J. Chem. Soc. Perkin Trans. 1998; 2:2141–2150.
94. Lewis DJ, Glover PB, Solomons MC, Pikramenou Z. J. Am. Chem. Soc. 2011; 133:1033–1043. [PubMed: 21182290]
95. Petoud S, Muller G, Moore EG, Xu J, Sokolnicki J, Riehl JP, Le UN, Cohen SM, Raymond KN. J. Am. Chem. Soc. 2007; 129:77–83. [PubMed: 17199285]
96. Hebbink GA, Reinhoudt DN, van Veggel FCJM. Eur. J. Org. Chem. 2001; 21:4101–4106.
97. Dickins RS, Howard JAK, Maupin CL, Moloney JM, Parker D, Riehl JP, Siligardi G, Williams JAG. Chem. Eur. J. 1999; 5:1095–1105.
98. Dickins RS, Howard JAK, Moloney JM, Parker D, Peacock RD, Siligardi G. Chem. Commun. 1997:1747–1748.
99. Walton JW, Di Bari L, Parker D, Pescitelli G, Puschmann H, Yufit DS. Chem. Commun. 2011; 47:12289–12291.

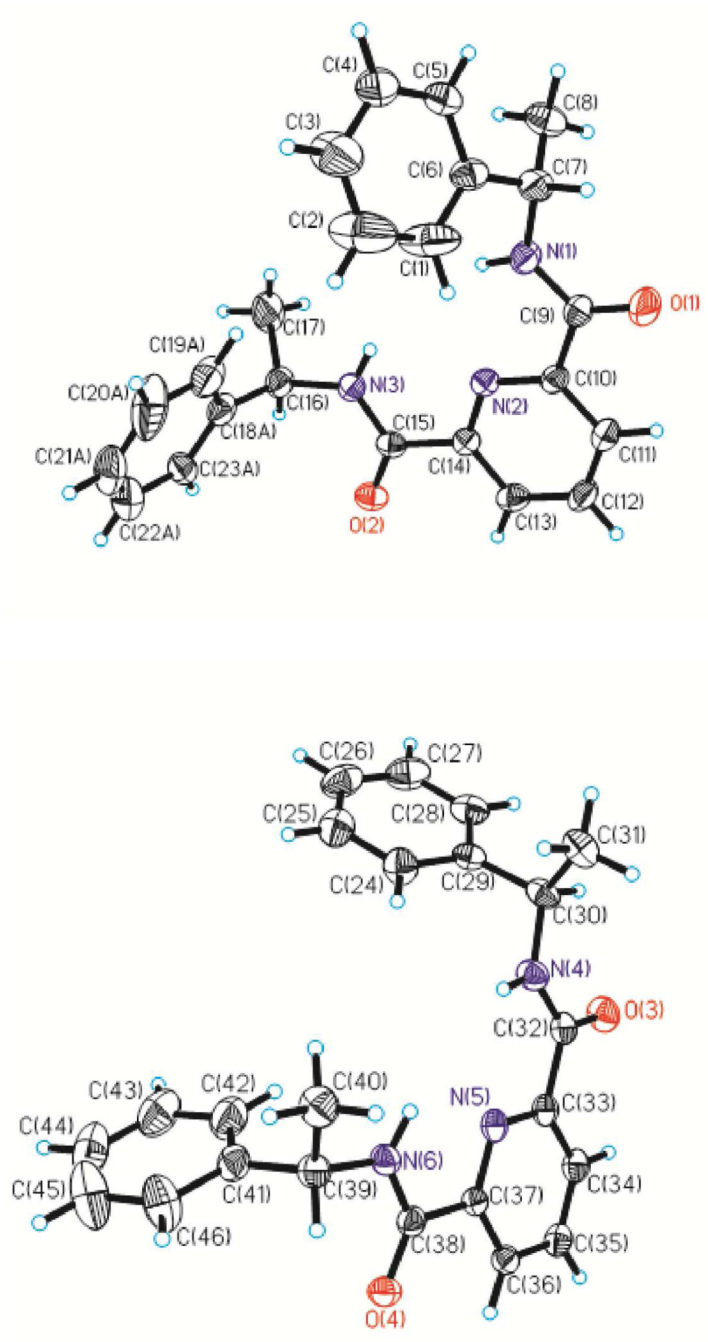

Figure 1.

Molecular structure and numbering scheme for the two types of (*R*,*S*)–**1** molecules found in the unit cell. Ellipsoids are represented with 50% probability.

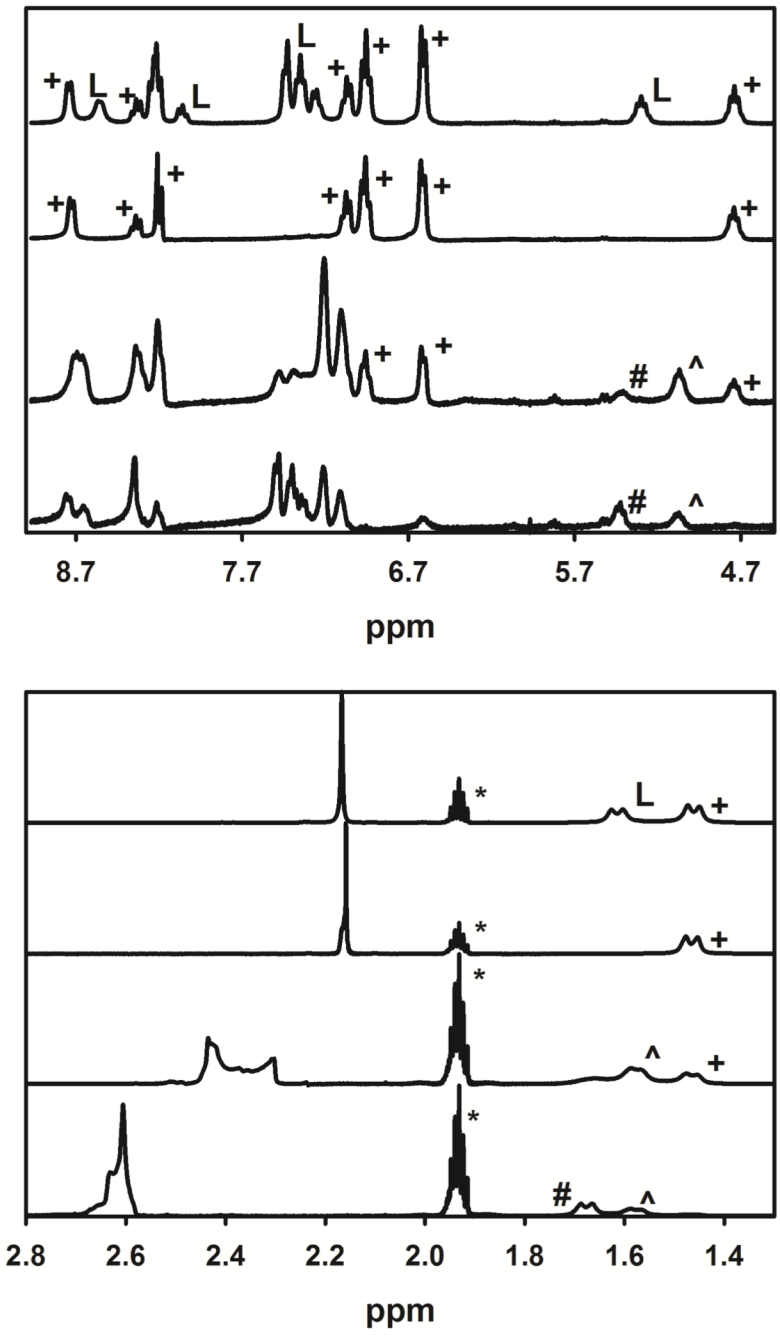

Figure 2.

^{1}H–NMR spectra of solutions containing various ratios, $R = [La]_t/[\mathbf{L}]_t$ of 0.2, 0.33, 0.5, and 1.0 (from top to bottom) in anhydrous CD_3CN (* symbol) at 298 K. The symbols **L**, #, ^, and + denote signals arising from the **L**, 1:1, 1:2, and 1:3 species, respectively. **L** = (*R*,*R*)–**1**).

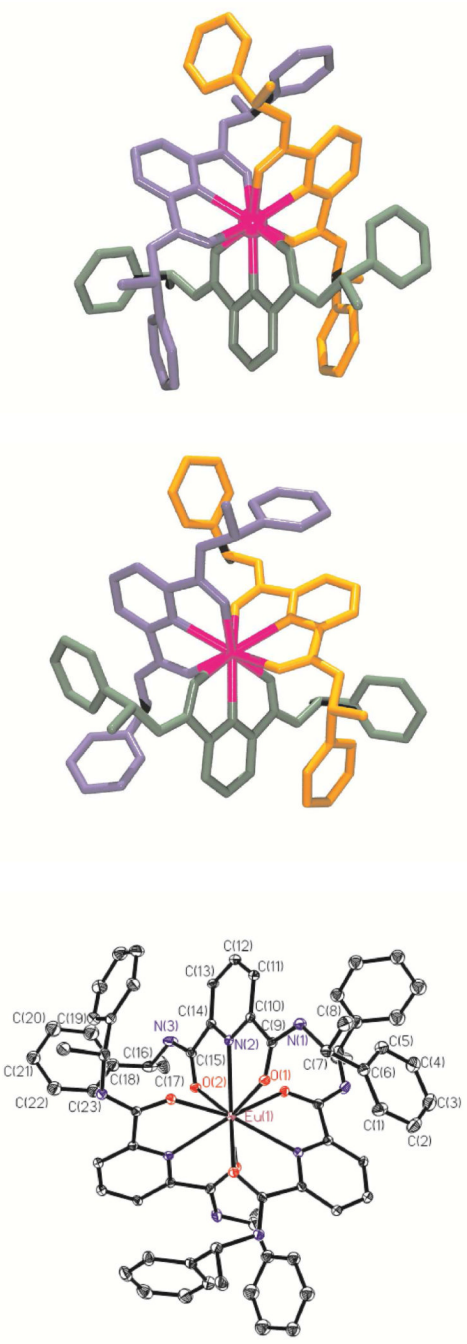

Figure 3.

Structure of the Λ–[Eu((*R*,*R*)–**1**)$_3$]$^{3+}$ (top) and Δ–[Eu((*S*,*S*)–**1**)$_3$]$^{3+}$ (middle) cations and atomic numbering scheme for Λ–[Eu((*R*,*R*)–**1**)$_3$]$^{3+}$ (bottom). Ellipsoids are represented with 50% probability.

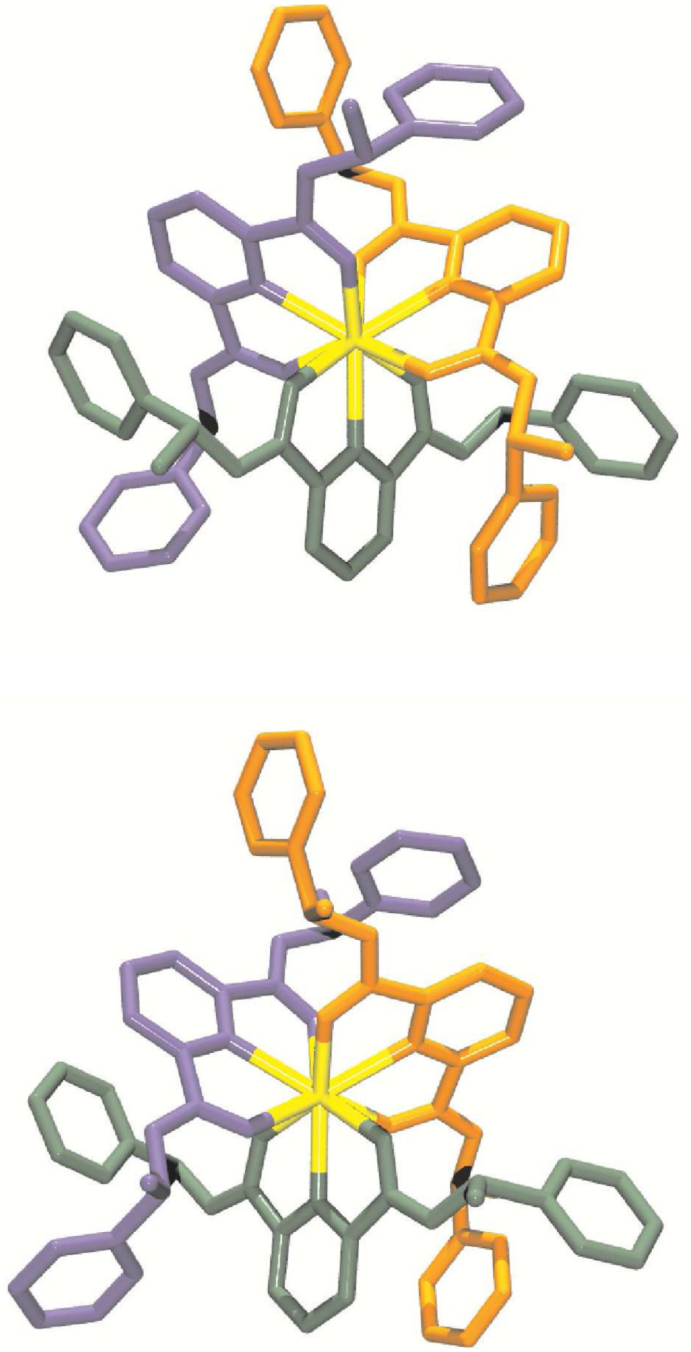

Figure 4.
Structure of the Λ–[Yb((*R*,*R*)–**1**)$_3$]$^{3+}$ (top) and Δ–[Yb((*S*,*S*)–**1**)$_3$]$^{3+}$ (bottom) cations.

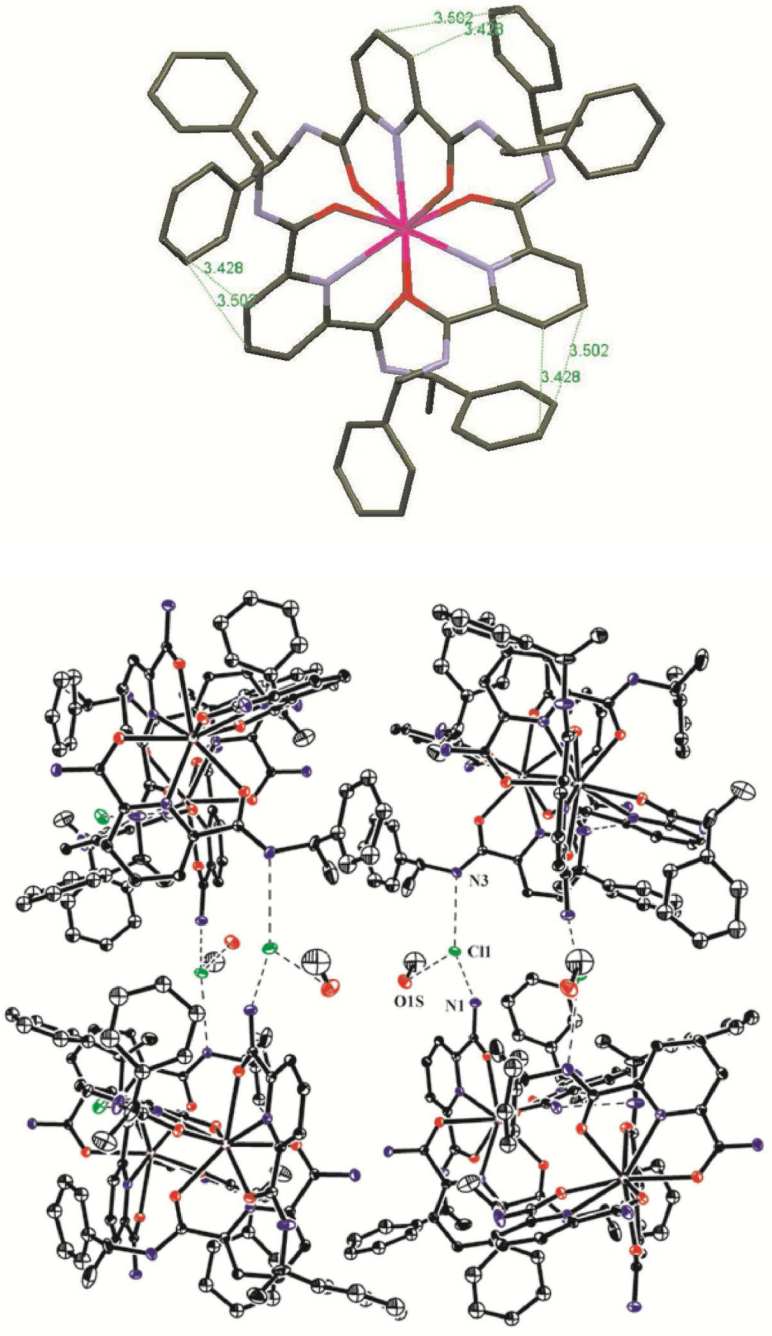

Figure 5.

Example of π–stacking interactions (top) and H–bonding interactions (bottom) observed in the crystal structure of the Λ–[Eu((*R*,*R*)–**1**)$_3$]$^{3+}$ cation. The distances for the Cl$^-$ anion H–bonded to N1, N3, and O1S are 3.172, 3.162, and 3.133Å, respectively. Ellipsoids are represented with 50% probability.

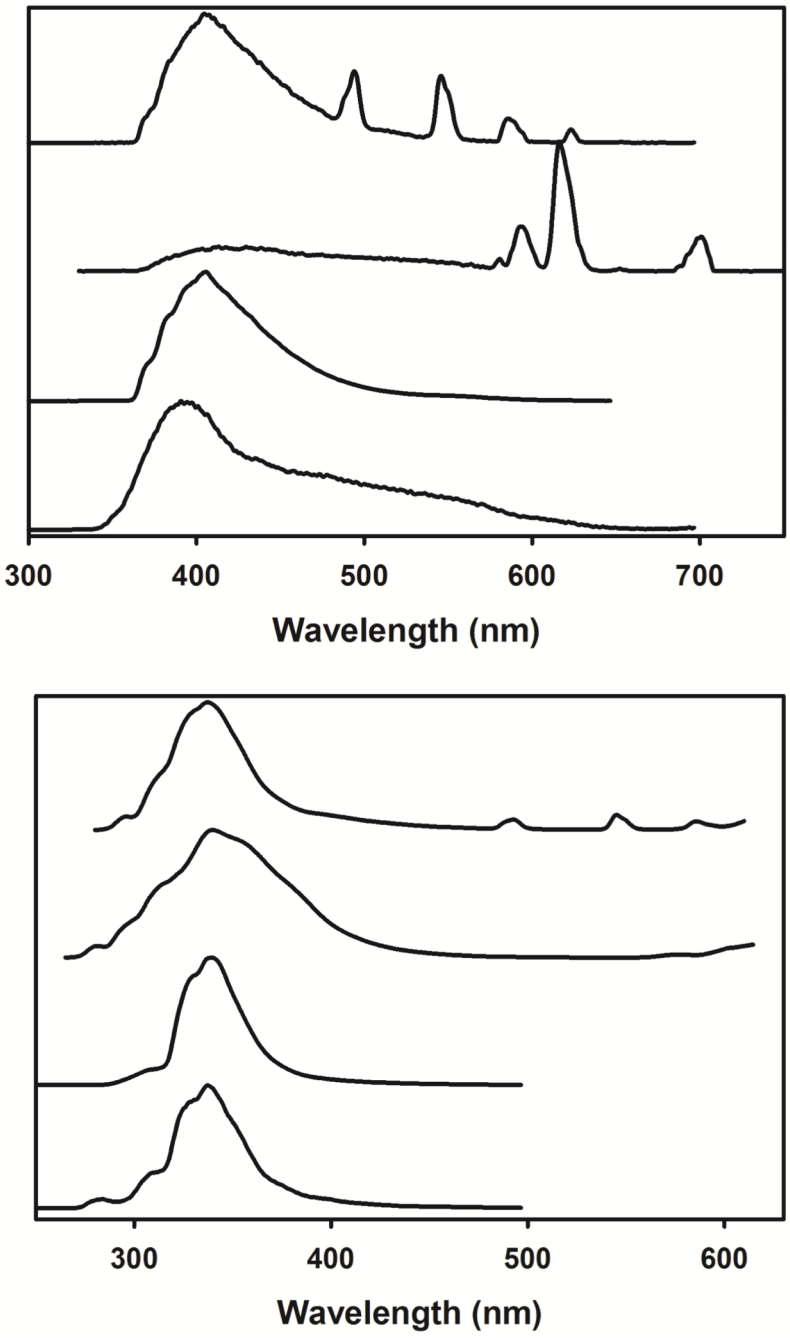

Figure 6.

Time–resolved (top) and steady–state (bottom) luminescence spectra of **L** and $[Ln\mathbf{L}_3]^{3+}$ in the solid state at 77 K (frozen MeCN solution) and in MeCN solution at RT, and recorded with time delays of 0.0 and 0.1 ms, respectively. From top to bottom: $[Ln\mathbf{L}_3]^{3+}$ (Ln(III) = Tb, Eu, and Gd) and **L**.

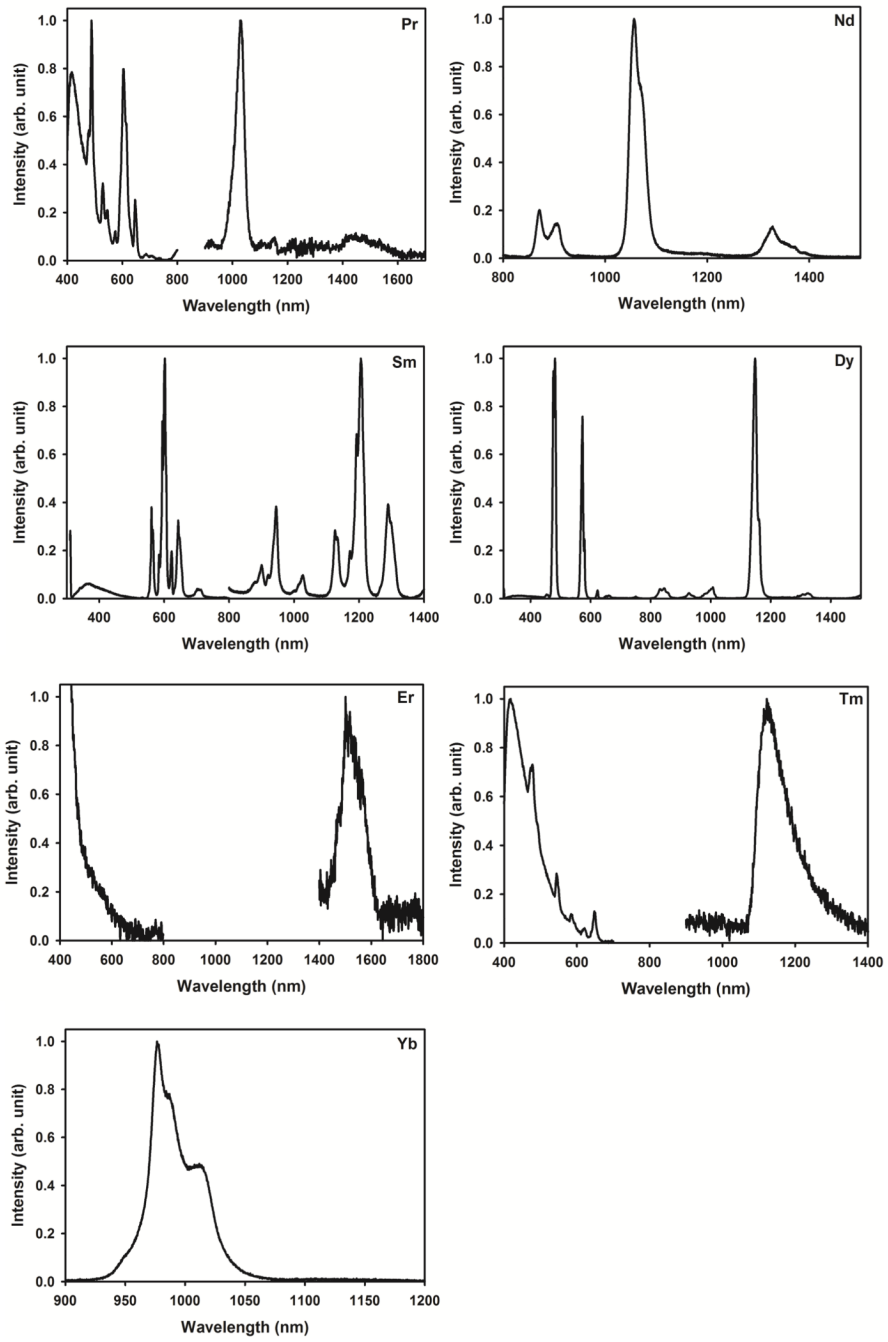

Figure 7.

VIS and NIR luminescence spectra of $[LnL_3]^{3+}$ (Ln(III) = Pr, Nd, Sm, Dy, Er, Tm, and Yb) in 6.7×10^{-3} M anhydrous MeCN at RT after excitation into the ligand–centered $n,\pi\rightarrow\pi^*$ transitions (λ_{exc} = 308 nm).

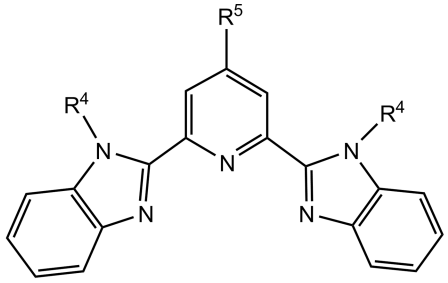

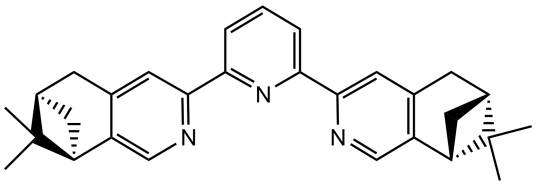

L^1

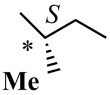

R^4 = * R^1 = Me

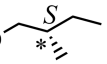

R^5 = H L^2

R^5 = COO * L^3

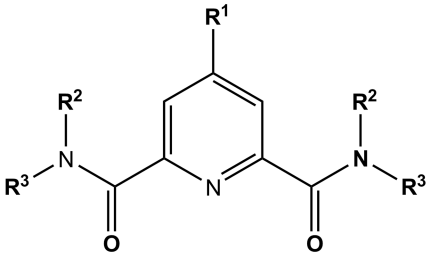

$R^1 = CH_2C^*H(CO_2Me)(NHCO_2CMe_3)$	$R^2 = R^3 = C_2H_5$	L^4
$R^1 = H$	$R^2 = R^3 = C_2H_5$	L^5
$R^1 = H$	$R^2 = R^3 = CH(CH_3)_2$	L^6
$R^1 = H$	$R^2 = R^3 = CH_2\text{-}C_6H_5$	L^7
$R^1 = H$	$R^2 = H$ $R^3 = CH_2\text{-}C_6H_5$	L^8
$R^1 = H$	$R^2 = H$ $R^3 = C_6H_5$	L^9

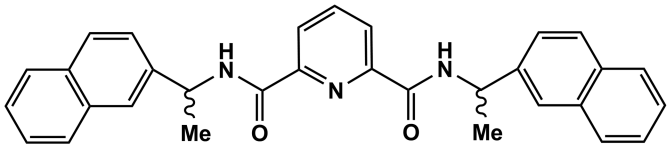

L' = (*R*,*R*)-1' and (*S*,*S*)-1'

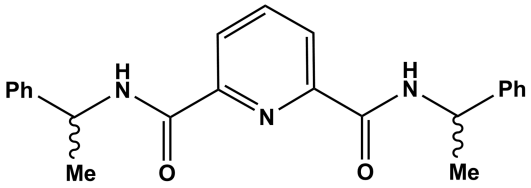

L = (*R*,*R*)-1, (*S*,*S*)-1, and (*R*,*S*)-1

Scheme 1.

Table 1

Crystallographic Data for (*R*,*S*)−**1** and $[Ln\mathbf{L}_3]^{3+}$ (Ln(III) = Eu, Yb and **L** = (*R*,*R*)−**1**)

	(*R*,*S*)−1	**$[EuL_3]^{3+}$**	**$[YbL_3]^{3+}$**
empirical formula	$C_{23}H_{23}N_3O_2$	$C_{70.5}H_{75}Cl_3EuN_9O_{7.5}$	$C_{70.5}H_{75.75}Cl_3N_9O_{7.88}Yb$
fw	373.44	1426.70	1454.54
T (K)	149(2)	153(2)	147(2)
cryst syst	orthorhombic	cubic	cubic
space group	$P2_12_12_1$	I23	I23
a/Å	10.053(4)	25.946(2)	25.839
b/Å	10.513(4)	25.946(2)	25.839
c/Å	37.598(16)	25.946(2)	25.839
α/deg	90	90	90
β/deg	90	90	90
γ/deg	90	90	90
V/Å^3	3974	17466	17251.5
Z	8	8	8
abs coeff (mm^{-1})	0.081	0.857	1.225
D_c/mg·m^{-3}	1.248	1.085	1.120
reflns collected	19008	43513	46664
unique reflns	4213	5338	6812
R_{int}	0.0536	0.0335	0.0384
params	560	274	276
final *R* [I > 2σ(*I*)]	0.0350	0.0298	0.0292
wR2	0.0594	0.0834	0.0787

Table 2

Species Observed in the ES–MS Spectra of Solutions ($[\mathbf{L}]_t = 2 \times 10^{-3}$ M in Anhydrous MeCN, **L** = (*R*,*R*)−**1**) with Ratios $R = [Eu]_t/[\mathbf{L}]_t = 0–4$ at 298 K.

Species	m/z[a]	Species	m/z[a]
$[(\mathbf{L}) + H]^+$	374.2	$[Eu(\mathbf{L})(NO_3)_2]^+$	650.1
$[(\mathbf{L}) + Na]^+$	396.2	$[Eu(\mathbf{L})_3(NO_3)]^{2+}$	667.2
$[Eu(\mathbf{L})_3]^{3+}$	424.2	$[2(\mathbf{L}) + Na]^+$	769.3
$[Eu(\mathbf{L})_2(NO_3)]^{2+}$	480.6	$[Eu(\mathbf{L})_2(NO_3)_2]^+$	1023.2
$[Eu(\mathbf{L})_4]^{3+}$	548.5	$[Eu(\mathbf{L})_3(NO_3)_2]^+$	1396.4

[a] *m/z* values given for the maximum of the peak at unit mass resolution.

Table 3

Cumulative Stability Constants of $[Eu(X)_n]^{3+}$ (n = 1–3 and X = **L**, $\mathbf{L}^i$ with i = 4–7) in anhydrous MeCN at 293 or 298 K.

X	Log β_1	Log β_2	Log β_3
L = (*R*,*R*)−**1**[a]	8.0(2)	15.9(2)	23.8(2)
$\mathbf{L}^4$ [b]	8.2(4)	14.6(5)	19.7(5)
$\mathbf{L}^5$ [c]	8.3(3)	15.3(3)	22.3(3)
$\mathbf{L}^6$ [d]	8.3(6)	13.9(6)	17.6(7)
$\mathbf{L}^7$ [d]	4.9(5)	9.8(6)	–

[a] Similar results were obtained for (*S*,*S*)−**1**.

[b] Taken from ref. 37.

[c] Taken from ref. 68.

[d] Taken from ref. 58.

Table 4

Selected Bond Lengths (Å) and Angles (deg) in $[LnL_3]^{3+}$ (Standard Deviation in Parentheses)

	$[EuL_3]^{3+}$ (L = (*R*,*R*)−1))			$[YbL_3]^{3+}$ (L = (*R*,*R*)−1))		
	Ligand	**Ligand #1**	**Ligand #2**	**Ligand**	**Ligand #1**	**Ligand #2**
			Bond Lengths			
Ln(1)-N(2)	2.564(2)	2.564(2)	2.564(2)	2.467(2)	2.467(2)	2.467(2)
Ln(1)-O(1)	2.397(2)	2.397(2)	2.397(2)	2.319(2)	2.319(2)	2.319(2)
Ln(1)-O(2)	2.397(2)	2.397(2)	2.397(2)	2.333(2)	2.333(2)	2.333(2)
			Bite angles N–Ln–N, O–Ln–N, and O–Ln–O			
N(2)-Ln(1)-N(2)#1		119.9(1)			120.0(1)	
N(2)-Ln(1)-N(2)#2		119.9(1)			120.0(1)	
N(2)#1-Ln(1)-N(2)#2		119.9(1)			120.0(1)	
O(1)-Ln(1)-N(2)#1		69.6(1)			138.5(1)	
O(2)-Ln(1)-N(2)#1		140.5(1)			69.8(1)	
O(1)-Ln(1)-N(2)#2		136.6(1)			72.8(1)	
O(2)-Ln(1)-N(2)#2		76.0(1)			137.6(1)	
O(1)#1-Ln(1)-N(2)		136.6(1)			72.7(1)	
O(2)#1-Ln(1)-N(2)		76.0(1)			137.6(1)	
O(1)#1-Ln(1)-N(2)#2		69.6(1)			138.5(1)	
O(2)#1-Ln(1)-N(2)#2		140.5(1)			69.8(1)	
O(1)#2-Ln(1)-N(2)		69.6(1)			138.5(1)	
O(2)#2-Ln(1)-N(2)		140.5(1)			69.8(1)	
O(1)#2-Ln(1)-N(2)#1		136.6(1)			72.7(1)	
O(2)#2-Ln(1)-N(2)#1		76.0(1)			137.6(1)	
O(1)-Ln(1)-O(1)#1		81.6(1)			79.9(1)	
O(1)-Ln(1)-O(1)#2		81.6(1)			79.9(1)	
O(1)-Ln(1)-O(2)#1		82.7(1)			142.6(1)	
O(1)-Ln(1)-O(2)#2		145.5(1)			83.9(1)	
O(2)-Ln(1)-O(1)#1		145.5(1)			83.9(1)	

	$[EuL_3]^{3+}$ (L = (*R*,*R*)−1))			$[YbL_3]^{3+}$ (L = (*R*,*R*)−1))		
	Ligand	**Ligand #1**	**Ligand #2**	**Ligand**	**Ligand #1**	**Ligand #2**
O(2)-Ln(1)-O(1)#2		82.7(1)		142.6(1)		
O(2)-Ln(1)-O(2)#1		82.1(1)		81.1(1)		
O(2)-Ln(1)-O(2)#2		82.1(1)		81.1(1)		
O(1)#1-Ln(1)-O(1)#2		81.6(1)		79.9(1)		
O(1)#1-Ln(1)-O(2)#2		82.7(1)		142.6(1)		
O(2)#1-Ln(1)-O(1)#2		145.5(1)		83.9(1)		
O(2)#1-Ln(1)-O(2)#2		82.1(1)		81.1(1)		

In addition to the formation of isostructural $[LnL_3]^{3+}$ complexes for the Ln(III) series studied (Eu–Yb) in the solid state, the introduction of a chiral asymmetric carbon in each carboxamide moiety led to a diastereomeric resolution of the 9–coordinate Ln(III) complexes. The ligand triplet–excited–state energy is relatively well suited to sensitize many Ln(III) ions emitting in the VIS and/or NIR regions.